ISPRS Journal of Photogrammetry and Remote Sensing 208 (2024) 245–260

Contents lists available at ScienceDirect

ISPRS Journal of Photogrammetry and Remote Sensing

journal homepage: www.elsevier.com/locate/isprsjprs

Open-set domain adaptation for scene classification using multi-adversarial learning

Juepeng Zheng [a], Yibin Wen [a], Mengxuan Chen [b,c], Shuai Yuan [d], Weijia Li [e,*], Yi Zhao [b,c], Wenzhao Wu [f], Lixian Zhang [b,c], Runmin Dong [b,c], Haohuan Fu [b,c,f,*]

[a] School of Artificial Intelligence, Sun Yat-Sen University, Zhuhai, China
[b] Ministry of Education Key Laboratory for Earth System Modeling, Department of Earth System Science, Tsinghua University, Beijing, China
[c] Tsinghua University (Department of Earth System Science)- Xi'an Institute of Surveying and Mapping Joint Research Center for Next-Generation Smart Mapping, Beijing, China
[d] Department of Geography, The University of Hong Kong, Hong Kong, China
[e] School of Geospatial Engineering and Science, Sun Yat-Sen University, Zhuhai, China
[f] National Supercomputing Center in Wuxi, Wuxi, China

ARTICLE INFO

Keywords:
Scene classification
Multi-adversarial learning
Remote sensing
Open-set domain adaptation
Negative transfer effect

ABSTRACT

Domain adaptation methods are able to transfer knowledge across different domains, tackling multi-sensor, multi-temporal or cross-regional remote sensing scenarios as they do not rely on labels or annotations in the target domain. However, most of the previous studies have focused on closed-set domain adaptation, based on the assumption that the source and target domains share identical class labels. Real-world scenarios are typically more complex, and the model could potentially encounter novel classes that are not previously included in the source domain, commonly referred to as "unknown" classes. Here we investigate the open-set domain adaptation scenario in the field of remote sensing scene classification, where there is a partial overlap between the label space of the target domain and that of the source domain. To deal with this problem, we propose a novel open-set domain adaptation method for scene classification using remote sensing images, which is named Multi-Adversarial Open-Set Domain Adaptation Network (MAOSDAN). Our proposed MAOSDAN consists of three main components. First, we employ an attention-aware Open Set BackPropagation (OSBP) to better distinguish the "unknown" and "known" samples for the target domain. Then, an auxiliary adversarial learning is designed for mitigating the negative transfer effect that arises from forcefully aligning the "unknown" target sample in network training. Finally, we adopt an adaptive entropy suppression to increase the probability of samples and prevent some samples from being mistakenly classified. Our proposed MAOSDAN achieves an average score of 75.07% in three publicly available remote sensing datasets, which significantly outperforms other open-set domain adaptation algorithms by attaining 4.52 ~ 17.15%. In addition, MAOSDAN surpasses the baseline deep learning model with 18.12% improvement. A comprehensive experimental evaluation demonstrates that our MAOSDAN shows promising prospects in addressing practical and general domain adaptation scenarios, especially in scenarios where the label set of the source domain is a subset of the target domain.

1. Introduction

In recent times, the remote sensing community has witnessed notable achievements through the effective utilization of deep learning techniques across various and multiple tasks, including geo-object detection (Zhu et al., 2017; Zou et al., 2017; Zheng et al., 2023), scene classification (Li et al., 2020b; Wang et al., 2020; Xu et al., 2021), and land cover mapping and land use mapping (Kussul et al., 2017; Hong et al., 2020). Image classification is in the majority in remote sensing field since deep learning algorithms can accept a variety of input predictor data with complex class signatures. However, the effectiveness of deep learning methods is highly dependent on the availability of large amounts of labeled data, as it operates in a data-centric manner (Liu et al., 2017, 2019; Rakshit et al., 2020; Zheng et al., 2021a). Furthermore, several algorithms have shown impressive results under the assumption that the training and testing data share similar feature space and distribution (Pan and Yang, 2009). Although in recent years,

* Corresponding authors.
E-mail addresses: liweij29@mail.sysu.edu.cn (W. Li), haohuan@tsinghua.edu.cn (H. Fu).

https://doi.org/10.1016/j.isprsjprs.2024.01.015
Received 13 June 2023; Received in revised form 6 December 2023; Accepted 16 January 2024
Available online 26 January 2024

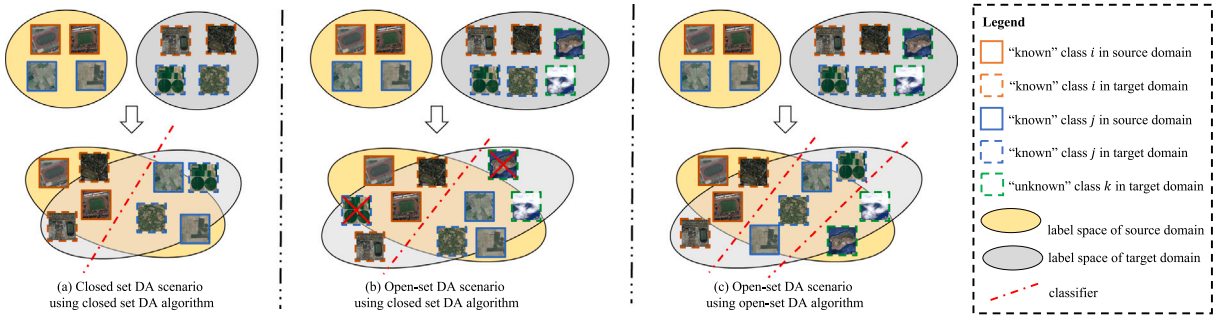

Fig. 1. Various DA scenarios. In the closed-set domain adaptation scenario, the assumption is made that the label sets are identical between the source and target domains, whereas in the open-set domain adaptation scenario, the label gap of the target domain encompasses that of the source domain. (a) Closed set DA scenario using closed set DA algorithm; (b) Open set DA scenario using closed set DA algorithm, which *cannot* distinguish "unknown" classes; (c) Open set DA scenario using open set DA algorithm, which distinguishes "unknown" class from common "known" classes.

the number of remote sensing images has rapidly increased and can be accessed via public, most of them remain unlabeled. Therefore, annotations for datasets are still required before applying deep learning algorithms, which is labor-exhausting and time-consuming. Besides this, it is hard for one to find exactly the same kind of images as the type of images used for a specific application (Panareda Busto and Gall, 2017). In many practical applications, images with the same annotations often share different distributions if they are acquired from different locations with different sensors. In this case, the model trained by the source data cannot be applied to the target data since deep learning algorithms will probably wrongly classify the images with different spatial resolutions and spectral distributions (Adayel et al., 2020). Therefore, narrowing the distribution disparity between the source and target domains to achieve more precise classification results becomes a necessity (Ye et al., 2017).

Fortunately, Domain Adaptation (DA) offers a solution by bridging the gap between the feature spaces of the source and target domains, enabling effective mapping from one domain to another (Panareda Busto and Gall, 2017). Existing DA approaches alleviate the domain distribution gap either via producing samples/features in target domains, or by representing domain invariant features, or by transferring samples across domains by generative networks. As shown in Fig. 1(a), most of them are closed-set DA, assuming that label sets are identical across source and target domains. However, the suppose of closed set DA may be easily violated owning to that real-world scenarios are usually more complicated in remote sensing applications. For example, it is easily accessible to acquire annotated tree species from different datasets. Nevertheless, if we want to recognize tree species in a brand new forest, we probably have to face two difficulties: (1) The variety of photographing conditions, acquisition time, sensors and environments lead to severe domain gap; (2) Some native tree species that ***donot*** exist in commonly accessible datasets lead to severe category gap, which denotes that the label set of source domain is a subset of the label set of target domain. In this paper, we refer to the situation where the label set of the source domain is encompassed within the label set of the target domain as open set DA. As shown in Fig. 1(b), if we adopt closed set DA approaches to complete open set DA scenarios, the model *cannot* distinguish "unknown" classes (native tree species). To this end, we add an "unknown" classes in the open-set DA algorithm to distinguish native tree species from common tree species in open-set DA scenarios (see Fig. 1(c)). In the remote sensing field, it is really common for open-set DA scenarios. For instance, in the task of land cover mapping, if we collect datasets of different types in various metropolis (e.g., Shanghai and New York) and want to transfer to a micropolis, such as Kashgar and Anchorage, there are some new land cover and land use types in micropolis that metropolis *donot* have (such as desert and tundra). Therefore, recognizing these "unknown" classes is quite vital in remote sensing applications, and an open-set DA algorithm can help us to better tackle this issue.

This paper introduces a novel open-set DA method, namely a Multi-Adversarial Open-Set Domain Adaptation Network (MAOSDAN), specifically designed for scene classification in remote sensing images, targeting situations where the label set of the source domain belongs to the target domain. The summary of our contributions is as follows:

1. We propose an open-set DA algorithm, named Multi-Adversarial Open-Set Domain Adaptation Network (MAOSDAN), for scene classification in remote sensing images to handle the open-set DA scenarios. Furthermore, the proposed MAOSDAN also demonstrates robustness on widely recognized open-set domain adaptation datasets within the computer vision community.
2. In our proposed MAOSDAN, we design an auxiliary adversarial classifier to evaluate the similarity of samples belonging to share label space, This auxiliary adversarial classifier effectively alleviates the negative transfer effect resulting from forcefully and mistakenly aligning those "unknown" target samples. We also improve the OSBP by an attention mechanism and design the adaptive entropy suppression in our proposed MAOSDAN.
3. We perform comprehensive experiments on three prominent remote sensing datasets, namely UC Merced, NWPU-RESISC45, and AID, to substantiate our findings. Our method showcases $4.52 \sim 17.15\%$ improvements in comparison to other state-of-the-art open-set DA algorithms and outperforms the baseline model by an improvement of 18.12%. Furthermore, we conduct a comprehensive analysis to identify and evaluate the adverse impact of existing closed-set and other open-set domain adaptation algorithms in open-set scenarios, specifically focusing on their performance in accurately classifying "unknown" target samples.

The remainder is structured as follows. In Section 2 the related works in the DA field are shortly surveyed. We present our elaborately-designed MAOSDAN methods in Section 3. We demonstrate our dataset and experiments in Section 4 and Section 5 respectively. In Section 6, we test the performance of our proposed model by analyzing the negative transfer effect and showing the feature visualization, and we conclude the article in Section 7.

2. Related work

2.1. Domain adaptation

Domain adaptation (DA) falls under the realm of transductive transfer learning, where the target and source tasks remain the same, but the domains differ (Pan and Yang, 2009). Categorized based on their approach to reducing domain shift, DA can be divided into three groups: discrepancy-based methods, adversarial methods, and self-supervised methods (Bucci et al., 2020). Discrepancy-based methods can measure the divergence between different domains, such as maximum mean

discrepancy (MMD) (Long et al., 2015, 2016; Zheng et al., 2021b), CORrelation Alignment (CORAL) (Sun et al., 2016) and Adaptive Feature Norm approach (Xu et al., 2019). Adversarial methods enable the harmonization of feature distributions between the source and target domains by leveraging a two-player minimax game Cao et al. (2018). Methods such as Generative Adversarial Network (GAN) (Goodfellow et al., 2014), BiGAN (Donahue et al., 2016), and conditional generative adversarial net (CGAN) (Mirza and Osindero, 2014) have been widely adopted in this research domain. Self-supervised learning learns useful feature representation by utilizing the data to train on artificial tasks for supervision (Bousmalis et al., 2016; Carlucci et al., 2019; Ghifary et al., 2016).

While the aforementioned methods show promising potential in reducing annotation efforts in the target domain, t is worth mentioning that the emphasis of these DA approaches lies predominantly on addressing the closed-set scenario, where the source and target domains have an identical label set. In this era of big data, real-world applications often exhibit a scenario where the label set in the target domain exceeds the label set in the source domain in terms of size. Hence, closed-set domain adaptation is no longer sufficient to address scenarios where an "unknown" class exists in the target domain. Therefore, it is imperative to shift our focus towards open-set domain adaptation scenarios, which better cater to these situations.

2.2. Open-set domain adaptation

Unlike closed-set domain adaptation, the inclusion of "unknown" classes in the target domain creates a divergence between the source and target domains. Although Panareda Busto and Gall (2017) firstly proposed the definition of open-set DA, it assumed that the source domain contains the "unknown" class, but it is not always a feasible way because it is difficult to define the contents of an "unknown" class in prior. To this end, Saito et al. (2018) proposed Open Set BackPropagation (OSBP) redefine the scenario where it does not need an "unknown" class sample in the source data. OSBP employs adversarial learning to effectively discriminate between unknown target samples and known target samples. Afterward, certain methods utilize a binary classifier to differentiate and exclude the unfamiliar samples from the target domain. Consequently, they solely align the known target samples with the source domain, leaving out the unknown instances (Feng et al., 2019; Liu et al., 2019; Shermin et al., 2020; Pan et al., 2020; Bucci et al., 2020; Jing et al., 2021; Kishida et al., 2021).

Existing open-set DA methods borrow the successful ideas from unsupervised DA algorithms and adapt them for open-set DA by tackling the unknown target samples in different ways. By utilizing existing adversarial learning techniques to discriminate between "known" and "unknown" target samples using a threshold, there is a potential risk of negative transfer effects. This approach unintentionally aligns target samples with "known" classes, leading to inaccurate classification results. Furthermore, we adopt an attention-aware OSBP and an adaptive entropy suppression to enhance the capability of transferability and confidence.

2.3. Domain adaptation in remote sensing

The manual annotation process for large datasets has become increasingly time-consuming and demanding due to the rapid expansion of remote sensing imagery. Therefore, an intriguing approach is to leverage pre-existing annotated remote sensing data to transfer knowledge from the labeled source domain to unlabeled target data. This method endeavors to utilize the knowledge from the labeled source domain to facilitate learning in the unlabeled target domain (Tuia et al., 2016b; Zhang et al., 2021c). The remote sensing data of the source and target domains can exhibit significant distribution gaps due to variations in sensors, geographic locations, photographing conditions, and other factors. As a result, in the remote sensing community, DA has been utilized to tackle long-time-series and large-scale applications by leveraging multi-temporal and multi-source remote sensing data, where the transferability of the model can be significantly influenced by variations in ground environments and imaging instruments (Tuia et al., 2016a). Until now, DA has proven to be effective in minimizing distribution gaps between remote sensing images and has found applications in various remote sensing tasks, including scene classification (Zhu et al., 2019; Lin et al., 2020; Ma et al., 2020; Kalita and Roy, 2020; Huang et al., 2023), object detection (Koga et al., 2020; Wu et al., 2020; Li et al., 2020a; Zhang et al., 2021b), semantic segmentation (Mateo-García et al., 2020; Shamsolmoali et al., 2020; Iqbal and Ali, 2020; Wittich and Rottensteiner, 2021; Lu et al., 2021; Vega et al., 2021; Li et al., 2021; Luo and Ji, 2022), 3D point cloud processing (Shen et al., 2023) and regression (Nyborg et al., 2022) tasks. DA approaches have been widely recognized as vital and effective in addressing the challenges of remote sensing-based multi-temporal, large-scale, and cross-regional scenarios.

The existing off-the-shelf DA approaches primarily focus on tackling the closed-set DA problem within the remote sensing community. Though in the remote sensing field some efforts have been made on a few more superior transfer-learning-based applications, such as multi-source DA (Elshamli et al., 2019), multi-target DA (Zheng et al., 2021c), partial DA (Hu et al., 2020; Zheng et al., 2022) and domain generalization (Zheng et al., 2021b), open-set DA is still lack of attention of researchers. There are several studies exploring open-set DA algorithms in remote sensing community (Adayel et al., 2020; Zhang et al., 2021a; Chen and Wang, 2022; Wang et al., 2023; Niu et al., 2023). Zhang et al. (2021a) minimizes both the overall distribution disparity between domains and the specific distribution differences among the same classes across different domains. But the performance of "unknown" class have no further improvement compared to other closed set DA methods (Zhang et al., 2021a). As for Adayel et al. (2020), by aligning the source and target domains and employing a pareto-based ranking scheme, it efficiently identifies potential samples belonging to the "unknown" class in the target domain. However, the accuracy of "unknown" samples is yet relatively low, some of which are even lower than 60%. Chen and Wang (2022) proposes MGCN to tackle open set few-shot scene classification issue, which is quite different from ours and it is a more specific scenario. We propose a new open-set domain adaptation method named MAOSDAN designed for scene classification in remote sensing images to especially strengthen the ability to recognize "unknown" target samples, addressing the challenging scenario encountered in real-world remote sensing applications. Furthermore, the proposed MAOSDAN is also robust on standard open-set DA datasets in the computer vision community.

3. Methodology

3.1. Preliminary and overview

First, we give notations and definitions before elaborating on our proposed approach. In the closed-set DA setting, there exists a source domain dataset ($D_s = \{(\mathbf{x}_i^s, y_i^s)\}_{i=1}^{n_s}$) with annotations and a label-free target domain dataset ($D_t = \{(\mathbf{x}_i^t)\}_{i=1}^{n_t}$) during the training phase, where n_s represents the number of images in the source domain dataset and n_t represents the number of images in the target domain dataset. Meanwhile, $\mathbf{x}_i^s$ represents a random sample in D_s and y_i^s denotes the matched annotation; $\mathbf{x}_i^t$ denotes a random sample in D_t without a known label. Notably, owing to the domain shift, feature distribution of the source domain ($P_s(\mathbf{x}^s, y^s)$) and the target domain ($P_t(\mathbf{x}^t)$) are commonly extremely diverse, meaning that applying the model trained on dataset D_s directly to evaluate dataset D_t can lead to significant performance deterioration. Moreover, in the context of open-set domain adaptation, it is important to note that the label set of the source data is a subset of the label set of the target data (i.e., $C_s \subseteq C_t$, where C_s and C_t represent the total number of classes in D_s and D_t, respectively). This

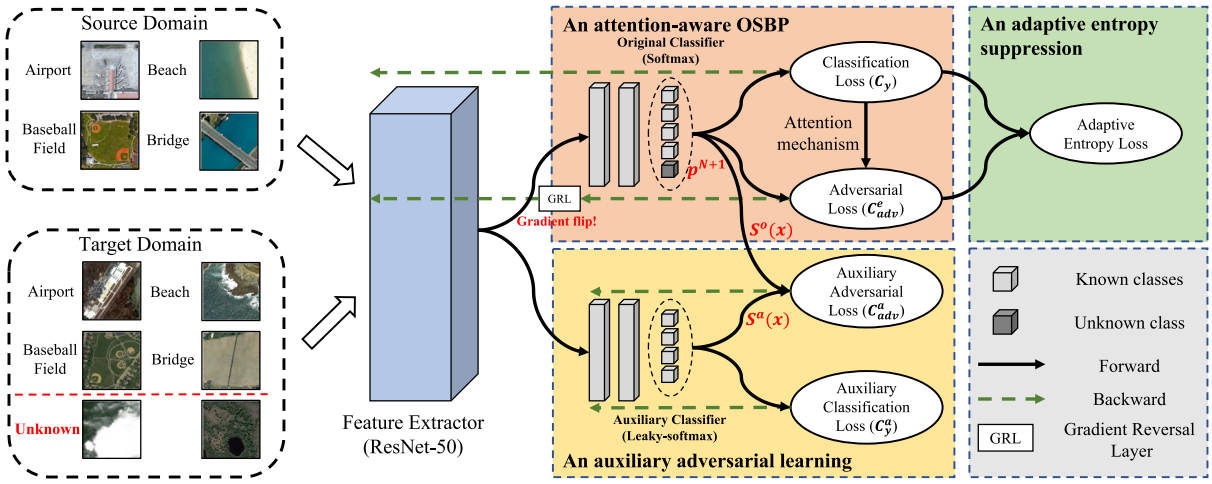

Fig. 2. The overall workflow of the proposed MAOSDAN. MAOSDAN contains three major modules, including an attention-aware Open Set BackproPagation (OSBP), an auxiliary classifier and an adaptive entropy suppression. An attention-aware OSBP: we modify the original OSBP (Saito et al., 2018) by assigning different weights in the adversarial module to better distinguish the unknown and known samples for the target domain; An auxiliary classifier: we design an auxiliary classifier with the same class outputs as the known classes, assisting our model to better align distributions between the source and the target domains and distinguish the unknown and known samples for the target domain; An adaptive entropy suppression: we propose an adaptive entropy suppression to enhance the prediction confidence and avoid forceful minimization of entropy value for the target domain through an attention mechanism.

setting meets wider applications in real-world scenarios, as we often have limited control over the class boundaries in the target domain. However, open-set DA scenarios present two significant challenges. One is that it is difficult to distinguish the "unknown" target samples from known ones while classifying the known target samples correctly; Another concern is the potential risk of directly aligning the global source distribution with that of the target domain as closed-set DA. The "unknown" target samples can negatively impact the performance of the DA model, potentially leading to worse results compared to a straightforward CNN model.

Therefore, we propose a new approach termed Multi-Adversarial Open Set Domain Adaptation Network (MAOSDAN), for open set remote sensing scene classification. Fig. 2 shows the overall workflow of our MAOSDAN, including three major modules, i.e., an attention-aware Open Set BackproPagation (OSBP), an auxiliary classifier and an adaptive entropy suppression. We summarized the three major components of MAOSDAN as follows:

1. An attention-aware OSBP. We modify the original OSBP (Saito et al., 2018) by assigning different weights in the adversarial module to better distinguish the "unknown" and "known" samples for the target domain. Those samples possessing high classification certainty are expected to own higher weights.
2. An auxiliary adversarial learning. We an auxiliary learning that shares the same class outputs as the known classes, aiding in effectively aligning the distributions between the source and target domains, as well as distinguishing between "unknown" and "known" samples within the target domain.
3. An adaptive entropy suppression. We propose an adaptive entropy suppression to enhance the prediction confidence and avoid forceful minimization of entropy value for the target domain through a weighting mechanism.

3.2. An attention-aware OSBP

Inspired by the minimax two-player game from Generative Adversarial Network (GAN) (Goodfellow et al., 2014) and Domain Adversarial Neural Network (DANN) (Ganin et al., 2016), OSBP develops a two-player game for open set domain adaptation problem, aiming at reducing the domain gap between the source and the target domains, as well as constructing a good boundary for the unknown class in the target domain (Saito et al., 2018). In general, the minimax game of OSBP can be formulated as:

$$\begin{aligned}\theta_g &= \arg\min_{\theta_g} C_y + C_{adv} \\ \theta_f &= \arg\min_{\theta_f} C_y - C_{adv}\end{aligned} \tag{1}$$

where θ_f and θ_g are the parameters of feature generator (G_f) and the classifier (G_y). The classifier G_y utilizes features generated by G_f to produce class probabilities in an $N+1$-dimensional space. Here, N represents the number of categories in the source domain, and the $(N+1)^{th}$ probability corresponds to the likelihood of the unknown class. In C_{adv}, a gradient reversal layer (Ganin et al., 2016) is employed to invert the gradient sign during the backward pass, allowing for effective domain alignment. C_y is the source classifier's objective, and C_{adv} is the adversarial objective, whose calculations are shown in Eqs. (2) and (3), respectively.

$$C_y\left(\theta_f,\theta_g\right) = \frac{1}{n_s}\sum_{\mathbf{x}_i\in D_s} L_y\left(G_y\left(G_f\left(\mathbf{x}_i\right)\right),y_i\right) \tag{2}$$

in which L_y denotes the classification loss calculated by the standard cross-entropy loss function.

$$\begin{aligned}C_{adv}\left(\theta_f,\theta_g\right) = &-\frac{1}{n_t}\sum_{\mathbf{x}_i\in D_t} t log\left(p\left(y=N+1|\mathbf{x}_i\right)\right) \\ &-\frac{1}{n_t}\sum_{\mathbf{x}_i\in D_t}(1-t)\,log\left(1-p\left(y=N+1|\mathbf{x}_i\right)\right)\end{aligned} \tag{3}$$

in which $p\left(y=N+1|\mathbf{x}_i\right)$ represents the probability of "unknown" class which can be formulated as $p\left(y=N+1|\mathbf{x}_i\right) = \left(G_y\left(G_f\left(\mathbf{x}_i\right)\right)\right)_{N+1}$. t is a constant value ($0<t<1$) that OSBP expects the output probability of the unknown class in the target domain. In the original paper (Saito et al., 2018), t is empirically equal to 0.5 to make a boundary between the known and the unknown target samples.

Because of its effectiveness and simplicity, OSBP has been adopted in other open set domain adaptation works (Feng et al., 2019; Shermin et al., 2020; Zhang et al., 2020). However, it seems unreasonable that it is identical for each sample from the target domain in the adversarial objective according to Eq. (3). The original OSBP may suffer from performance degradation due to the presence of "hard" samples, which are located in the classifier's margin. Especially in remote sensing scene classification tasks, it is very common that samples of two different classes have similar texture and spectral characteristics, such as Bare

Land and Dessert, Grassland and Farmland, Overpass and Intersection, etc. To this end, there are many similar samples that are "hard" to classify in remote sensing field. Consequently, the adversarial learning process is expected to assign lower weights to the "hard" samples and higher weights to the "easy" samples. We quantify how the sample is "hard" or "easy" by the entropy criterion $H(h) = -\sum_{n=1}^{N} h_n log\left(h_n\right)$, also employ an entropy-based weighting scheme $m(\mathbf{x}) = 1 + e^{-H(h(\mathbf{x}))}$ on each target sample (Long et al., 2018). Therefore, our improved adversarial objective in OSBP can be calculated as Eq. (4).

$$\begin{aligned} C_{adv}^{e}\left(\theta_f, \theta_g\right) = & -\frac{1}{n_t} \sum_{\mathbf{x}_i \in D_t} m\left(\mathbf{x}_i\right) t log\left(p\left(y = N+1 | \mathbf{x}_i\right)\right) \\ & - \frac{1}{n_t} \sum_{\mathbf{x}_i \in D_t} m\left(\mathbf{x}_i\right)(1-t) log\left(1 - p\left(y = N+1 | \mathbf{x}_i\right)\right) \end{aligned} \tag{4}$$

3.3. An auxiliary adversarial learning

Although our improved OSBP addresses the imbalanced problem for "hard" and "easy" samples, it remains unavoidable negative transfer effects. OSBP attempts to align those samples with $p(y = N+1) < 0.5$ in the target domain, which are considered as "known" class. However, no all target samples with $p(y = N+1) < 0.5$ should be considered as "known" class. For example, when the probability of an "unknown" class for a target sample is $p(y = N+1) = 0.45$ while the probabilities of other "known" classes are all lower than 0.45, forcefully aligning this target sample to the known classes may cause negative transfer effect. Therefore, we add an auxiliary classifier to extend the domain adversarial module and reduce the negative transfer effect. In remote senisng community, it is quite difficult to recognize brand-new scenarios ("unknown" class), especially for land use mapping. For example, if the "commercial" is an "unknown" class and the "dense residential" is one of the known classes. It is easily to recognize the "commercial" as "dense residential" instead of "unknown" class. Furthermore, if we use previous popular open-set domain adaptation methods that heavily depends on a fixed threshold from utilizing existing adversarial learning techniques to discriminate between "known" and "unknown" target samples (Saito et al., 2018; Feng et al., 2019), the adaptation model could not recognize "unknown" samples correctly and also cause deterioration of "known" classes to some extent. To this end, we propose an auxiliary adversarial learning to solve the above limitations.

Different from the original classifier, our auxiliary classifier outputs N probabilities for each training sample. The source training samples can be accurately classified into N classes through our auxiliary classifier, which better learns the representations of the "known" classes. Therefore, besides the original classification objective in Eq. (2), we have auxiliary classification objective (C_y^a), which can be formulated as Eq. (5):

$$C_y^a\left(\theta_f, \theta_g^a\right) = \frac{1}{n_s} \sum_{\mathbf{x}_i \in D_s} L_y\left(G_y^a\left(G_f\left(\mathbf{x}_i\right)\right), y_i\right) \tag{5}$$

in which θ_g^a denotes the parameters of the auxiliary classifier (G_y^a). Notably, we adopt a leaky-softmax (Cao et al., 2019) in the auxiliary domain classifier to ensure that the total probability of known classes is less 1. To this end, we have two kinds of probabilities to describe the similarity between the training samples and the "known" classes, i.e., $S^o(\mathbf{x})$ and $S^a(\mathbf{x})$, which are induced by the original classifier and the auxiliary classifier and can be calculated as Eq. (6):

$$\begin{aligned} S^o(\mathbf{x}) &= 1 - p(y = N+1 | \mathbf{x}) \\ S^a(\mathbf{x}) &= \sum_{k=1}^{N} G_y^{a,k}\left(G_f(\mathbf{x})\right) \end{aligned} \tag{6}$$

We integrate these two probabilities to finally measure the similarity ($S(\mathbf{x})$) of training samples belonging to share label space according to Eq. (7). Specially, if the training samples are classified as the "known" class, the value of $S(\mathbf{x})$ will be high or close to 1, while if the training samples *do not* belong to share label space, the value of $S(\mathbf{x})$ will be low or close to 0. It should be emphasized that once one of these two similarity measures is low, the final similarity $S(\mathbf{x})$ will have a low value, indicating the training sample is dissimilar to the "known" class. This strategy indicates that our auxiliary classifier can enhance the capacity of distinguishing the samples belonging to "unknown" classes.

$$S(\mathbf{x}) = S^o(\mathbf{x}) \times S^a(\mathbf{x}) \tag{7}$$

Therefore, our auxiliary domain adversarial objective can be formulated as Eq. (8):

$$\begin{aligned} C_{adv}^{a}\left(\theta_f, \theta_g^a\right) = & -\frac{1}{n_s} \sum_{\mathbf{x}_i \in D_s} log\left(S\left(\mathbf{x}_i\right)\right) \\ & - \frac{1}{n_t} \sum_{\mathbf{x}_i \in D_t} log\left(1 - S\left(\mathbf{x}_i\right)\right) \end{aligned} \tag{8}$$

3.4. An adaptive entropy suppression

To enhance the prediction confidence of classifier in semi-supervised learning, entropy minimization regularization is proposed (Grandvalet and Bengio, 2004) and have been widely used in DA algorithms for modifying the adaptive classifier (Long et al., 2016; Zheng et al., 2020). Entropy loss is a method developed to improve the confidence of classifier predictions based on the entropy function derived from information theory. This approach aims to increase the classifier's ability to effectively utilize unlabeled samples in the target domain. More specifically, entropy suppression regularization reduces the uncertainty of probability distributions for output categories. Nevertheless, entropy is *not* needed to be minimized for all samples in the target domain. For example, it is difficult to recognize the input samples into "known" or "unknown" samples. Negative consequences may arise when attempting to forcefully minimize the entropy of these target samples that pose challenges in accurate classification. In addition, due to different sensors and surface environment, the spectral and texture characteristics for remote sensing images of the same class can be quite different. Therefore, the prediction from the classifier for the target remote sensing images may have low prediction scores for correct classes. To this end, we propose an adaptive entropy suppression, which is proposed to reduce the uncertainty of probabilities for output classes, to make the classifier more accessible to the unlabeled target remote sensing images. We can adopt the output of original classifier $\hat{y}_i = G_y\left(G_f\left(\mathbf{x}_i\right)\right)$ to generate a weight for each target sample's entropy suppression, only utilizing the probability of "unknown" prediction confidence. The value of weight can be formulated as Eq. (9):

$$\begin{aligned} v_i &= 1 - [p^{N+1} log\left(p^{N+1}\right) + \left(1 - p^{N+1}\right) log\left(\left(1 - p^{N+1}\right)\right)] \\ p^{N+1} &= p\left(y = N+1 | \mathbf{x}_i\right) \end{aligned} \tag{9}$$

We can easily understand that the more transferable the corresponding sample is, the larger the attention value v_i is. Our attentive entropy regularization is employed to embed the entropy-guidance attention value v_i into the entropy loss, which can be calculated as:

$$\begin{aligned} C_{\text{ent}}\left(\theta_f, \theta_g\right) = & -\frac{1}{n_s} \sum_{\mathbf{x}_i \in D_s} \sum_{c=1}^{N} \cdot p_i^c \cdot \log\left(p_i^c\right) \\ & - \frac{1}{n_t} \sum_{\mathbf{x}_i \in D_t} \sum_{c=1}^{N+1} v_i \cdot p_i^c \cdot \log\left(p_i^c\right) \end{aligned} \tag{10}$$

where N means the amount of classes, and p_i^c denotes the prediction likelihood of classifier for sample $\mathbf{x}_i$ corresponding to class c, and we can get them by calculating from $\mathbf{p}_i = G_y\left(G_f\left(\mathbf{x}_i\right)\right)$. In this way, the adaptive entropy suppression improves the certainty and confidence of the prediction, thus effectively improving the classifier's performance.

Table 1
The detailed information of three common and available remote sensing datasets.

Dataset	Year	Classes	Images per class	Number of images	Resolution (m)	Size	Source
NWPU-RESISC45	2017	45	700	31,500	0.2~30	256 × 256	Google Earth
AID	2017	31	220~420	10,000	0.5~8	600 × 600	Google Earth
UC Merced	2010	21	100	2,100	0.3	256 × 256	USGS

Table 2
The label information for the five transfer tasks is provided below. The class names within parentheses represent the corresponding class names in the target domain. It is important to note that shared classes are present in both the source and target domains, whereas unknown classes are exclusive to the target domain and are collectively considered as "unknown" classes. It is worth mentioning that we have excluded the scenario of NWPU-RESISC45 → UC Merced, as all the classes in UC Merced are already included in NWPU-RESISC45.

Source domain	Target domain	Shared classes	Unknown classes
AID	NWPU-RESISC45	Bridge, Baseball field, Church, Beach, Forest, Airport, Medium residential, Dense residential, Desert, Commercial Rectangular Farmland, Circular Farmland Industrial, Port (Harbor),Ground track field Storage tank, Sparse residential, Meadow, Viaduct (Overpass) River, Mountain, Stadium, Railway station, Parking	Chaparral, Basketball Court, Cloud, Airplane Lake, Palace, Mobile Home Park, Island Intersection, Golf Course, Freeway Runway, Railway, Sea Ice, Roundabout Tennis Court, Snowberg, Terrace, Ship Thermal Power Station, Wetland
AID	UC Merced	Baseball field, Beach, Commercial (Buildings), Parking, Medium residential, Port (Harbor), Forest Sparse residential, Viaduct (Overpass), Storage tanks Farmland (Agricultural), River, Dense residential	Chaparral, Golf Course, Freeway, Intersection Runway, Tennis Court, Mobile Home Park, Airplane
NWPU-RESISC45	AID	Beach, Church, Airport, Commercial area, Baseball diamond Circular farmland & Rectangular farmland (Farmland), River, Medium residential, Harbor (Port), Sparse residential Dense residential, Industrial area, Parking lot, Mountain Forest, Railway station, Meadow, Ground track field Storage tank, Stadium, Desert, Viaduct, Bridge	School, Resort, Pond, Square Center, Bare Land, Park
UC Merced	AID	Baseball diamond, Farmland, Buildings (Commercial), Forest, Meadow, Medium residential, Park, Dense residential Sparse residential, River, Harbor (Port), Parking lot, Storage tanks	Church, Bridge, Center, Airport, Square, Bare Land Desert, Industrial, Overpass (Viaduct), Mountain, Beach, Stadium, Playground, Resort, Pond, School, Railway Station
UC Merced	NWPU-RESISC45	Baseball diamond, Airplane, Buildings (Commercial), Beach Agricultural (Circular farmland & Rectangle farmland), Freeway Golf course, Intersection, Medium residential, Harbor Parking lot, Mobile home park, River, Chaparral, Runway, Forest Overpass, Tennis court, Sparse residential, Storage tanks	Bridge, Basketball Court, Cloud, Church, Airport Industrial Area, Ground Track Field, Island, Meadow, Palace, Railway, Railway Station, Roundabout, Snowberg, Ship, Sea Ice, Terrace, Stadium, Lake, Thermal Power Station, Wetland, Mountain, Desert

3.5. Minimax optimization problem

Therefore, our proposed MAOSDAN consists of an attention-aware OSBP, an auxiliary classifier loss and an adaptive entropy suppression. Our minimax optimization issue aims to find the parameters of model θ_f, θ_g and θ_g^e that satisfy as Eq. (11) jointly:

$$\begin{aligned}\hat{\theta}_g &= \arg\min_{\theta_g} C_y + \lambda C^e_{adv} \\ \hat{\theta}_f &= \arg\min_{\theta_f} C_y - \lambda C^e_{adv} + \alpha\left(C^a_y - \beta C^a_{adv}\right) + \gamma C_{ent} \\ \hat{\theta}^e_g &= \arg\min_{\theta^e_g} C^a_y + \beta C^a_{adv}\end{aligned} \tag{11}$$

where C_{adv} and C_{y} denote the domain adversarial alignment and the classification's learning objective for the source domain, respectively. C^a_{y} and C^a_{adv} mean the auxiliary classifier's learning objective and the domain adversarial objective of the auxiliary classifier, respectively. In addition, C_{ent} denotes the entropy loss. λ, β, α and γ denote three hyper-parameters to manually realize trade-off among different objectives.

4. Datasets

To assess and measure the effectiveness of our novel MAOSDAN approach, we curate a unique dataset by combining three distinct open-source remote sensing datasets (i.e., NWPU-RESISC45 (Cheng et al., 2017), AID (Xia et al., 2017) and UC Merced (Yang and Newsam, 2010)), which are originated from various regions and different sensors with diverse resolutions and acquisition dates. Table 1 lists the thorough details of used open-source datasets. These datasets have been utilized for validating previous domain adaptation approaches in remote sensing field (Lu et al., 2019; Liu and Su, 2020; Adayel et al., 2020; Zhu et al., 2021). Firstly, we review these three remote sensing datasets. Then we present our re-organized and re-collected dataset and finally introduce our open set domain adaptation scenarios.

- **NWPU-RESISC45** (Cheng et al., 2017) comprises a total of 31,500 images, with each image having a spatial resolution ranging from 30 m to 0.2 m per pixel. These images are classified into 45 distinct scene classes, with each class consisting of 700 images. Notably, this dataset stands out as the largest among the three datasets used in this paper. It is characterized by its remarkable between-class similarity, significant within-class diversity, and a wide range of image variations.
- **AID** (Xia et al., 2017) is composed of 30 aerial scene categories obtained from the Google Earth platform. Each class in the dataset includes sample images collected from diverse regions and countries, captured during different seasons, times, and imaging conditions. The AID dataset comprises a collection of 10,000 sample images, with varying class sizes ranging from 220 to 420 images. Each image in the AID dataset has dimensions of 600 × 600 pixels.
- **UC Merced** (Yang and Newsam, 2010) encompasses a diverse range of 21 land use classes, obtained from high-resolution aerial orthoimagery with a pixel resolution of one foot. This dataset has garnered considerable acclaim as a valuable asset for scene classification endeavors in the field of remote sensing. It has

Fig. 3. Examples of five open-set domain adaptation scenarios: AID → NWPU-RESISC45, AID → UC Merced, NWPU-RESISC45 → AID, UC Merced → AID, and UC Merced → NWPU-RESISC45. It is worth noting that we exclude the NWPU-RESISC45 → UC Merced scenario, as all the classes in UC Merced are already present in NWPU-RESISC45.

emerged as a pioneering open-source validation dataset, serving as an important benchmark for evaluating various methods and techniques. The images within the UC Merced dataset have been extracted from large-scale aerial images obtained from the United States Geological Survey (USGS).

Based on the class composition of NWPU-RESISC45, AID, and UC Merced datasets, we have devised five distinct transfer scenarios for our study. The label information for each scenario is presented in Table 2. It is notable that the transfer task from NWPU-RESISC45 to UC Merced represents a typical domain adaptation scenario, as categories in the UC Merced dataset already exist in the NWPU-RESISC45 dataset. Thus, we have a total of five transfer tasks for open-set domain adaptation across these three datasets. Please note that the class names provided in parentheses in Table 2 indicate their respective names in the target domain. For instance, in the UC Merced → NWPU-RESISC45 transfer task, the class "Agricultural" in UC Merced matches the classes "Rectangular Farmland" and "Circular Farmland" in NWPU-RESISC45. Similarly, in the AID → NWPU-RESISC45 transfer task, the class "Port" in AID matches the class "Harbor" in NWPU-RESISC45. As we can observe, the more "unknown" classes there are, the more difficult the transfer task becomes. Fig. 3 showcases some representative classes from these five transfer tasks, highlighting the open-set DA scenarios involved.

5. Experiments

5.1. Setup

In our experimental setup, we set the values of three hyperparameters, namely λ, α, β, and γ, as 1.0, 0.1, 2.0, and 1.0, respectively. All the experiments were performed using PyTorch (Paszke et al., 2019) using GeForce 2080 Ti. The ResNet-50 model architecture (He et al., 2016) serves as the backbone for our model and is initially pre-trained on the ImageNet dataset (Russakovsky et al., 2015). In our approach, we utilize a learning rate of 0.001 and follow the annealing strategy outlined in the work of Ganin et al. (2016). As for the optimizer, we use mini-batch stochastic gradient descent (SGD) (Bottou, 2010) as our optimizer incorporating a momentum of 0.9. The batch size used in our experiments is set to 36. Our proposed MAOSDAN and other approaches are evaluated by our re-organized datasets introduced in Section 4. Five types of open set DA scenarios are conducted for each method. The five transfer tasks are **U** → **N**, **A** → **N**, **A** → **U**, **U** → **A**, and **N** → **A**, in which **A**, **U** and **N** represent AID, UC Merced, and NWPU-RESISC45 respectively. Our codes are available in https://github.com/rs-dl/MAOSDAN. We hope that our open-source codes could promote the development of open-set domain adaptation and its applications in remote sensing community.

To keep consistency with previous studies (Loghmani et al., 2020; Bucci et al., 2020), We employ a set of four evaluation metrics to assess the performance of our approach. These metrics include: (1) OS, which represents the normalized accuracy across all classes, including the unknown class; (2) OS^*, which measures the normalized accuracy specifically for the known classes; (3) UNK, indicating the accuracy of the unknown samples; and (4) HOS, which represents the harmonic mean of OS^* and UNK and which can be formulated as Eq. (12). In the metrics of open-set DA scenario, OS is a measure of the overall performance combining with OS^* and UNK. However, including UNK as a separate class does not offer a suitable solution. It becomes particularly problematic when the number of known classes increases, as the impact on open-set recognition becomes more pronounced. In such cases, the role of the UNK class becomes insignificant and fails to adequately capture the true performance of the system. In this study, we will prioritize the utilization of the HOS metric, which holds significant importance. This decision stems from its ability to assess the algorithm's performance on both known and unknown samples, rendering it a comprehensive evaluation criterion.

$$HOS = 2 \times \frac{OS^* \times UNK}{OS^* + UNK} \tag{12}$$

5.2. Experimental results

We compare our MAOSDAN with five cutting-edge open-set DA algorithms, including OSBP (Saito et al., 2018), STA (Liu et al., 2019), DAMC (Shermin et al., 2020), Unknown-Aware Domain Adversarial Learning (UADAL) (Jang et al., 2022) and Self-Supervised-driven Open-set Unsupervised Domain Adaptation (SSOUDA) (Wang et al., 2023). OSBP employs adversarial learning to distinguish between unknown target samples and known target samples. STA employs a progressive weighting mechanism to effectively distinguish between samples belonging to unknown and known classes, while also assigning importance to their contribution in aligning feature distributions. On the other hand, DAMC incorporates a weighting module that assesses the unique domain characteristics to assign representative weights to target samples, facilitating positive transfers during adversarial training. UADAL (Jang et al., 2022) aligns the source and the target-known distribution while simultaneously segregating the target-unknown distribution in the feature alignment procedure. SSOUDA (Wang et al., 2023) combines contrastive self-supervised learning with consistency self-training for optical remote sensing scene classification and retrieval, obtaining reliable unknown class samples for co-training. Additionally, we conduct a comparative analysis between our proposed method, MAOSDAN, and six widely recognized DA approaches. The six standard DA approaches includes Joint Adaptation Network (JAN) (Long et al., 2017), Domain Adaptation Network (DAN) (Long et al., 2015), Domain Adversarial Neural Network (DANN) (Ganin et al., 2016), Conditional Domain Adaptation Network (CDAN) (Long et al., 2018),

Table 3
Performance metrics on our collected dataset for open-set DA scenarios (ResNet-50):OS, OS*, UNK and HOS (%).

Method		Standard domain adaptation							Open-set domain adaptation					
		ResNet-50	JAN	DAN	DANN	CDAN	DALN	PCLUDA	STA	OSBP	DAMC	UADAL	SSOUDA	MAOSDAN
A→N	OS	56.43	56.72	59.24	60.86	57.15	50.56	49.63	63.13	71.20	59.30	62.66	55.28	**73.82**
	OS^*	55.97	56.41	59.25	60.79	56.66	49.61	49.41	63.02	71.29	58.46	60.82	54.73	**74.52**
	UNK	66.89	63.72	59.04	62.50	68.39	72.42	54.59	65.51	57.53	**78.73**	68.09	67.93	73.17
	HOS	60.95	59.85	59.14	61.63	61.98	58.88	51.87	64.24	63.88	67.09	64.25	60.62	**73.84**
A→U	OS	56.80	62.44	65.70	66.80	72.95	58.21	64.88	66.40	71.64	67.88	75.04	67.96	**78.20**
	OS^*	55.39	63.15	65.39	67.00	73.08	57.54	66.23	65.62	72.15	66.46	75.17	70.23	**78.46**
	UNK	75.25	53.13	69.75	64.25	71.25	67.00	47.38	76.63	65.00	**86.25**	73.33	38.37	85.63
	HOS	63.81	57.71	67.50	65.60	72.15	61.91	55.24	70.69	68.39	75.07	74.24	49.63	**79.17**
N→A	OS	61.01	72.86	73.21	76.47	70.68	67.03	78.21	63.86	79.07	71.34	73.99	73.07	**80.24**
	OS^*	60.45	72.87	73.31	76.59	70.46	66.79	78.53	62.63	79.04	70.36	72.57	73.03	**80.46**
	UNK	73.94	72.57	71.02	73.63	75.75	72.43	70.80	**92.04**	79.69	88.76	78.86	73.81	89.20
	HOS	66.52	72.72	72.14	75.08	73.01	69.50	74.46	74.54	79.37	78.50	75.58	73.41	**82.23**
U→A	OS	35.76	59.66	48.61	60.72	52.86	37.08	**70.85**	53.77	66.85	60.59	56.97	58.24	68.03
	OS^*	34.47	60.41	48.63	60.70	52.68	34.30	**72.85**	51.67	66.76	58.91	55.69	59.21	67.82
	UNK	52.61	49.78	50.51	60.90	55.16	73.30	44.83	81.14	68.07	82.50	58.27	45.69	**83.56**
	HOS	41.65	54.58	49.47	60.80	53.89	46.73	55.50	63.13	67.41	68.73	56.95	51.58	**74.87**
U→N	OS	44.88	45.42	50.43	49.50	49.14	40.33	49.47	46.11	60.59	54.28	52.55	61.06	**61.45**
	OS^*	44.02	44.48	50.18	48.97	48.19	38.60	49.33	44.86	60.44	53.12	51.22	**61.65**	61.08
	UNK	63.03	65.07	55.58	60.53	69.01	76.60	52.44	72.44	63.70	**78.48**	72.14	48.63	76.10
	HOS	51.84	52.84	52.74	54.14	56.75	51.33	50.84	55.41	62.03	63.36	59.91	54.37	**65.26**
Avg	OS	50.98	59.42	59.44	62.87	60.55	50.64	62.61	58.65	69.87	62.68	64.14	63.12	**72.36**
	OS^*	50.06	59.47	59.32	62.81	60.21	49.37	63.27	57.56	70.04	61.46	63.09	63.77	**72.47**
	UNK	66.34	60.85	61.18	64.36	67.91	72.35	54.01	77.55	66.80	**82.94**	70.14	54.89	81.53
	HOS	56.95	59.54	60.20	63.45	63.56	57.67	57.58	65.60	68.21	70.55	66.43	57.92	**75.07**

Table 4
The efficiency of different DA methods (ResNet-50).

Method	Number of parameters (M)	GFLOPs	Inference time (ms per image)
ResNet-50	49.31	5.40	1.22
DAN	49.31	5.40	1.34
JAN	49.31	5.40	1.38
DANN	50.57	50.57	1.28
CDAN	60.33	6.03	1.28
STA	51.83	5.96	2.64
OSBP	49.31	5.40	1.29
DAMC	50.57	5.81	1.44
MAOSDAN (Ours)	50.57	5.81	1.32

Discriminator-free Adversarial Learning network (DALN) (Chen et al., 2022), Pseudo-label Consistency Learning-based Unsupervised Domain Adaptation (PCLUDA) (Hou et al., 2022). JAN focuses on aligning the joint distributions of multiple domain-specific layers using a joint maximum mean discrepancy. DAN employs an optimal multi-kernel selection method to reduce the domain discrepancy through mean embedding matching. DANN, in contrast, leverages a gradient reversal layer to facilitate adaptation, but it may not effectively discriminate between the source and target domains. Another approach, Deep Coral adopts a linear transformation for aligning the statistical distributions of the source and target domains. On the other hand, CDAN incorporates multilinear conditioning and entropy conditioning as two conditioning strategies in its architecture. DALN (Chen et al., 2022) reuses the category classifier as a discriminator, which achieves explicit domain alignment and category separation through a unified objective, enabling the DALN to leverage the predicted discriminative information for sufficient feature alignment. PCLUDA (Hou et al., 2022) minimizes the difference in probability distribution between the target domain and its perturbed output by a pseudo-label self-training and consistency regularization strategy, followed by adjusting the target domain's decision boundaries to the low-density region. In Table 3, in addition, we include the Baseline (ResNet-50 (He et al., 2016)) model in our evaluation, which serves as a reference point for comparison. It should be emphasized that the Baseline model exclusively utilizes classification loss without incorporating any domain adaptation techniques.

Table 3 presents the evaluation results of our dataset in five transfer tasks for open-set domain adaptation, utilizing ResNet-50 as the backbone model. As for the standard DA methods, CDAN (Long et al., 2018) performs best in terms of HOS, with 6.61% higher than the Baseline (a straight forward ResNet-50 model). Most of standard DA methods achieve improvement, while some of them still lower than the Baseline. For example, the HOS of PCLUDA, JAN and DALN are lower than the Baseline in the task of **A** → **U** with −8.57%, −6.10%, −1.90%, respectively. The UNK of JAN, DAN, DANN, DALN and PCLUDA are lower than the Baseline in the task of **N** → **A** with −1.37%, −2.92%, −0.31%, −1.51% and −3.14%, respectively. The outcomes obtained from standard DA methods highlight the presence of significant adverse transfer effects in open-set DA scenarios (refer to Section 5.4 for more information). As for open-set DA algorithms, our proposed MAOSDAN attains the highest average HOS of 73.08%, with 4.52% to 17.15% improvement compared to other three open-set DA methods. Our MAOSDAN also shows superior HOS on each transfer tasks except **U** → **A**. In addition, MAOSDAN attains 18.12% gains compared to the Baseline in terms of HOS. On the other hand, DAMC (Liu et al., 2019) perform best in UNK with an average accuracy of 82.94%, and its UNK achieve higher score than our proposed MAOSDAN with regards of **A** → **N**, **A** → **U** and **U** → **N** three tasks. However, its OS^* is relatively lower than MAOSDAN (over -10%).

Furthermore, we list the efficiency (including the number of parameters, the FLOPs (floating point of operations) and the inference time (ms per image)) of different DA methods using ResNet-50 in Table 4. Obviously, our proposed MAOSDAN is comparable with other existing DA methods in efficiency and model size, while achieves the best performance among them (See Table 3).

5.3. Ablation studies

Here, we present the performance analysis (HOS) of various experiments conducted on our custom dataset for our novel MAOSDAN approach, utilizing ResNet-50 as the backbone architecture. The ablation studies in Table 5 examine the contributions of different components, namely A-OSBP, AAL, and AES, which correspond to attention-aware OSBP, auxiliary adversarial learning, and adaptive entropy suppression, respectively. It is worth mentioning that the Baseline method

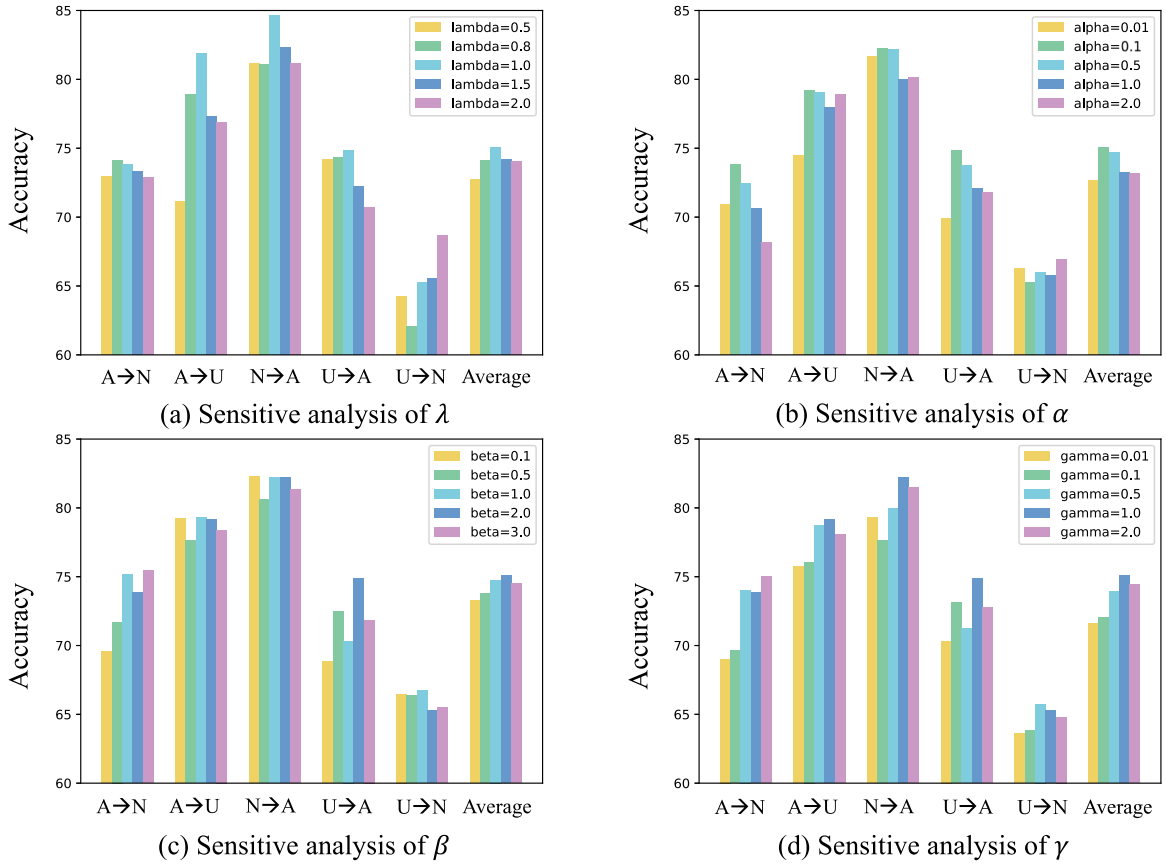

Fig. 4. The accuracy (%) of MAOSDAN for our collected dataset in open-set DA scenarios under different hyper-parameters of λ, α, β and γ.

Table 5
The performance (%) of HOS on our collected dataset for the ablation studies of our proposed method (ResNet-50).

A-OSBP	AAL	AES	A → N	A → U	N → A	U → A	U → N	Avg
×	×	×	63.88	68.39	79.37	67.41	62.03	68.21
✓	×	×	67.78	74.71	80.21	71.02	64.71	71.67
×	✓	×	65.04	76.56	77.76	69.60	62.68	70.33
×	×	✓	70.10	71.57	77.12	69.97	63.50	70.45
✓	✓	×	69.44	78.17	80.50	70.24	**66.03**	72.88
✓	×	✓	73.27	**79.36**	82.19	72.70	65.34	74.57
×	✓	✓	72.98	77.37	76.44	74.33	64.89	73.20
✓	✓	✓	**73.84**	79.17	**82.23**	**74.87**	65.26	**75.07**

(represented in the first row of Table 5) refers to the initial OSBP approach (Saito et al., 2018) as described in Eq. (1).

5.3.1. The effectiveness of the A-OSBP

In contrast to the original OSBP, our enhanced OSBP incorporates a novel re-weighting mechanism designed to enhance performance in open-set domain adaptation scenarios. Additionally, our attention-aware mechanism yields a significant improvement of 3.46% when compared to the original OSBP. It is observable that our attention-aware OSBP considerably increase the classification accuracy in challenging transfer tasks, demonstrating remarkable performance improvements, such as **A** → **N** (+3.90%), which has more "unknown" classes in the target domain. Furthermore, the attention-aware OSBP achieves +2.55%, +4.12% and +1.87% respectively on the basis of AAL, AES and AAL + AUS and with respect to the average HOS.

5.3.2. The effectiveness of the AAL

In contrast to prior approaches for open-set DA methods (Saito et al., 2018; Kishida et al., 2021), we propose an auxiliary classifier to mitigate the negative transfer caused by "unknown" target samples. As shown in Table 5, our AAL performs +2.12% better than OSBP, especially attaining significant improvement on **A** → **U** (+8.17%). In addition, the AAL achieves +1.21%, +2.75% and +0.50% improvements respectively on the basis of A-OSBP, AES and A-OSBP + AUS with respect to the average HOS.

5.3.3. The effectiveness of the AES

We introduce adaptive entropy suppression, which serves two purposes: firstly, it improves the confidence of classification probabilities for output classes, contributing to the classifier being more interpretable for target data without annotations; secondly, it prevents the forced minimization of entropy for "unknown" samples that pose challenges in recognition. From Table 5, we can see that though the performance drops on the transfer task of **N** → **A** (−2.25%), our adaptive entropy suppression increase the average HOS of +2.24%. In addition, the adaptive entropy suppression yields +2.90%, +2.87% and +2.19% increment respectively based on A-OSBP, AAL and A-OSBP + AAL with the respect of the average HOS.

5.3.4. Sensitive analysis

In this section, we conducted comprehensive ablation studies on four crucial hyperparameters: λ, α, β, and γ. The performance of our proposed MAOSDAN on our dataset, specifically in open-set domain adaptation scenarios, was evaluated. Notably, we select the hyperparameters that achieve the highest average HOS metric for all transfer tasks. Fig. 4 illustrates the results of the HOS metric corresponding to the variations of these hyperparameters, as shown in Fig. 4. When $\alpha = 0.1$, $\beta = 2.0$ and $\gamma = 1.0$, we assess a range of values for the parameter λ, varying from 0.5 to 2.0, in our evaluation (Fig. 4(a)). It has been observed that the setting $\lambda = 1.0$ outperforms other configurations, demonstrating a noticeable improvement. Specifically, when $\lambda = 1.0$,

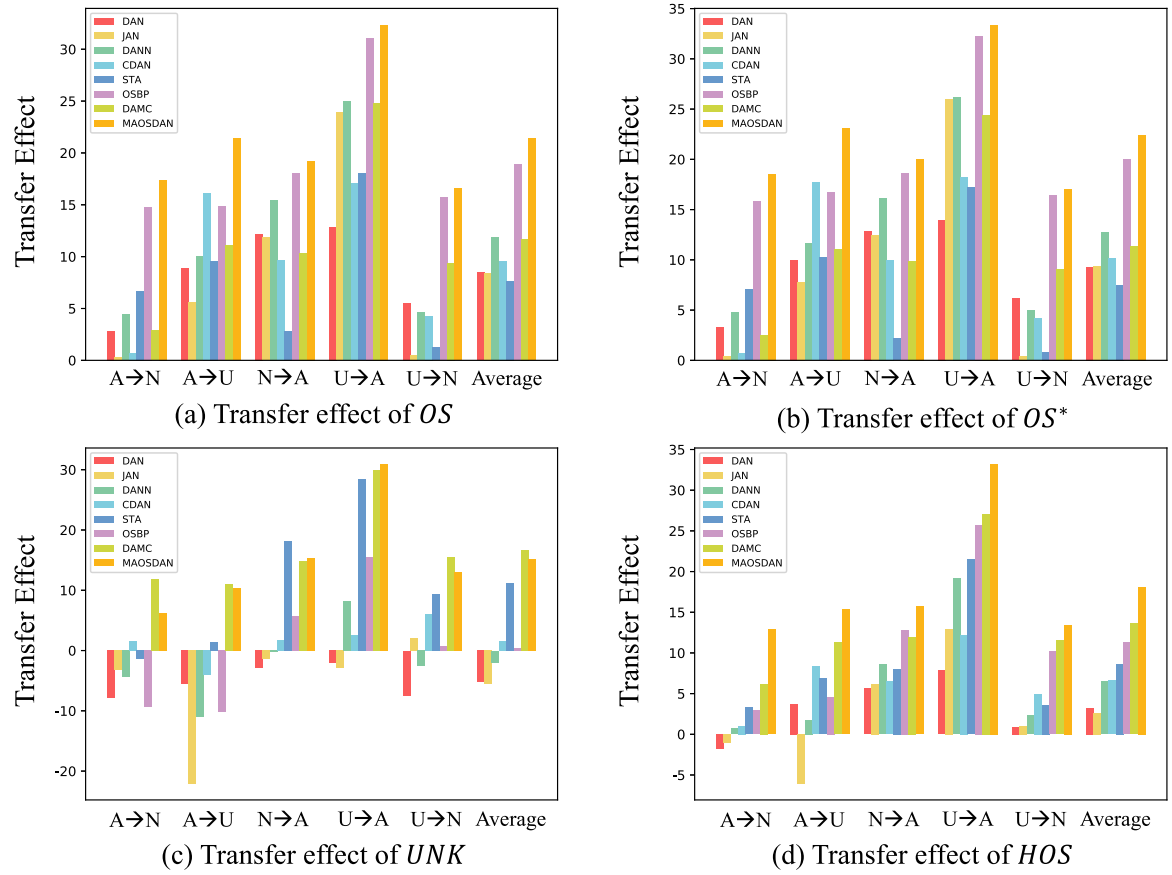

Fig. 5. The transfer effect (%) of different DA methods for our collected dataset in open-set DA scenario.

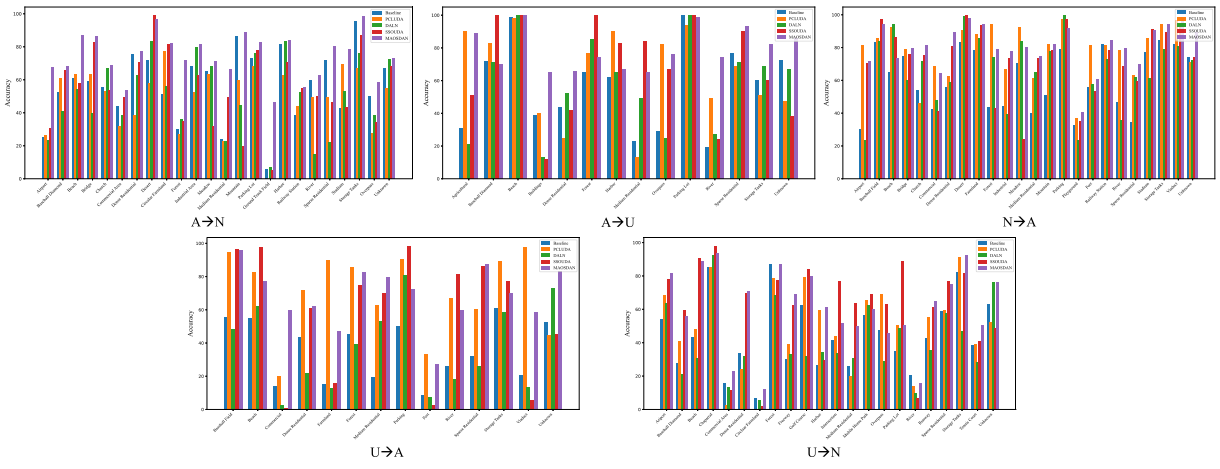

Fig. 6. The accuracy (%) of each class for five different methods (including ResNet-50, PCLUDA, DALN, SSOUDA and MAOSDAN) for all transfer tasks. (For interpretation of the references to color in this figure legend, the reader is referred to the web version of this article.)

$\beta = 2.0$, and $\gamma = 1.0$, the evaluation is conducted across various values of α, ranging from 0.01 to 2.0 (refer to Fig. 4(b)). It is observable that when the $\alpha < 0.1$, the accuracy dramatically drops. In addition, the HOS of $\alpha = 1.0$ is slightly higher than $\alpha = 0.5$. When $\lambda = 1.0$, $\alpha = 0.1$ and $\gamma = 1.0$, we assess the influence of β with different values ranging from 0.1 to 3.0 (Fig. 4(c)). We find that there is little difference among the performance of different β values, while the HOS of $\beta = 2.0$ is slightly higher than others. Finally, a sensitivity analysis is conducted on various values of γ, ranging from 0.01 to 2.0, while keeping $\lambda = 1.0$, $\alpha = 0.1$, and $\beta = 2.0$ fixed. Fig. 4(d) reveals that accuracy significantly drops when $\gamma < 1.0$, and the HOS of $\gamma = 1.0$ is slightly higher than that of $\gamma = 2.0$. Based on these findings, we establish a set of balanced hyperparameters for all our experiments: $\lambda = 1.0$, $\alpha = 0.1$, $\beta = 2.0$, and $\gamma = 1.0$. This ensures consistent and reliable results across our study, avoiding any potential bias or inconsistency.

5.4. Transfer effect

In this part, we point out the positive transfer effect proxies for aforementioned DA approaches, and deeply analysis whether there exists the negative transfer effect, especially for the closed set DA approaches in UNK of the open-set DA problem. The Negative Transfer

Table 6
The performance (%) of HOS on different backbones along with different open-set algorithms.

Backbones	Methods	A → N	A → U	N → A	U → A	U → N	Avg
ResNet-50	Baseline	60.95	63.81	66.52	41.65	51.84	56.95
	DANN	61.63	65.60	75.08	60.80	54.14	63.45
	OSBP	63.88	68.39	79.37	67.41	62.03	68.21
	MAOSDAN	**73.84**	**79.17**	**82.23**	**74.87**	**65.26**	**75.07**
ResNet-101	Baseline	60.10	65.22	69.42	52.23	53.06	60.01
	DANN	63.27	68.15	76.50	61.90	54.39	64.84
	OSBP	62.55	68.00	58.97	64.31	59.33	62.63
	MAOSDAN	**68.78**	**70.95**	**79.56**	**65.89**	**64.14**	**69.86**
ResNeXt-101	Baseline	77.04	64.14	71.18	54.67	54.53	64.31
	DANN	65.34	70.68	77.72	61.98	58.00	66.74
	OSBP	75.10	**76.86**	**78.82**	72.87	**66.63**	74.06
	MAOSDAN	**79.68**	75.66	78.68	**73.85**	66.31	**74.84**
EfficientNet	Baseline	61.12	67.69	74.03	52.88	52.94	61.73
	DANN	64.39	68.24	78.90	59.05	57.62	65.64
	OSBP	66.16	74.77	**79.39**	63.13	63.82	69.45
	MAOSDAN	**68.85**	**75.82**	76.37	**64.06**	**64.20**	**69.86**

Effect (NTE) describes the transferability of the trained model compared to the Baseline method (a straight forward deep learning model, i.e., ResNet-50), which only utilizes the source domain data without any DA strategies. Therefore, the NTE can be calculated as:

$$\mathrm{NTE} = \mathrm{ACC}_{\mathrm{OSDA}} - \mathrm{ACC}_{\mathrm{Baseline}} \tag{13}$$

where $\mathrm{ACC}_{\mathrm{OSDA}}$ and $\mathrm{ACC}_{\mathrm{Baseline}}$ are the performance (such as OS, OS^*, UNK and HOS) of the open set DA methods and the Baseline method. If the value of NTE is greater than zero, it indicates that the DA method demonstrates a positive transfer impact in the open-set DA scenarios. On the contrary, NTE < 0 represents the DA method results in a NTE in the open set DA scenario not only without any improvement but with accuracy deterioration. Fig. 5 presents the performance evaluation of the NTE metric for various DA methods, encompassing both closed-set and open-set approaches. It is convincing and easy-understand that all of DA methods achieve positive transfer effect in terms of OS and OS^* (as shown in Fig. 5(a) and (b)) since they minimize the domain gap between the source and the target domains. However, as for the evaluation of UNK (see Fig. 5(c)), three closed DA methods including DAN, JAN and DANN encounter severe NTE ranging from -1.98% to -5.49%. In the task of **A** → **U**, all closed set DA methods suffer from NTE in terms of UNK, with $-4.00\% \sim -22.13\%$. In addition, OSBP is also confronted with NTE. In the task of **A** → **N**, two open set DA algorithms are both prone to the NTE problem in terms of UNK, which indicates that general open set DA methods are not sure to gain improvement in remote sensing applications. Owning to the positive effect generated from OS^*, the average scores of HOS (see Fig. 5(d)) are all better than the Baseline except some NTE cases in the tasks of **A** → **N** and **A** → **U**. Our proposed MAOSDAN yields the highest transfer effect in all four evaluations, with $+21.38\%$, $+22.41\%$, $+15.19\%$ and $+18.12\%$ for OS, OS^*, UNK and HOS, respectively. To this end, directly adopting closed DA approaches will result in relatively severe performance deficiency in the open set DA tasks, especially for the accuracy of UNK. Our experiments also prove the necessity for our proposed components introduced in Section 3 in MAOSDAN to prevent from the negative transfer effect in open set DA scenarios.

6. Discussion

6.1. The performance of different classes

Here we discuss the performance of each class instead of only presenting overall accuracy. Fig. 6 displays the accuracy (%) of each class for five different methods (including ResNet-50 (He et al., 2016), PCLUDA (Hou et al., 2022), DALN (Chen et al., 2022), SSOUDA (Wang et al., 2023) and MAOSDAN) for all transfer tasks. We can observe that the accuracy of "unknown" class outperforms other methods with considerably gains (the purple bar of the last group in each figure in Fig. 6). However, the accuracies of "known" classes for MAOSDAN are not always higher than other methods. For example, in the transfer task of **U→N**, the accuracy of MAOSDAN is lower than that of SSOUDA (Wang et al., 2023) for "Baseball Diamond", "Mobile Home Park", "Intersection" and "Chaparral". As a matter of fact, the accuracy of "known" classes (OS^*) and "unknown" class (UNK) are two key factors to evaluate the effectiveness of open-set scenarios. Usually, the higher accuracy of "known" classes means the lower accuracy of "unknown" class, while the higher accuracy of "unknown" class means the lower accuracy of "known" classes. To this end, we adopt the harmonic mean of OS^* and UNK to represent the ability of the algorithm's performance on both known and "unknown" samples. From Table 3, our proposed MAOSDAN achieves the highest average HOS compared to other SOTA methods.

6.2. The performance of different backbones and image degradation along with our proposed MAOSDAN

In this paper, we actually focus on designing the better open-set domain adaptation algorithm using multi-adversarial learning. We hope that our proposed MAOSDAN could perform higher classification accuracy (including both "known" classes and the "unknown" class). Our MAOSDAN is a plug-and-play algorithm that could easily applied to other network architectures. In addition, we list different network architectures along with our proposed MAOSDAN in open-set domain adaptation scenarios for all transfer tasks, including ResNet-50 (He et al., 2016), ResNet-101 (He et al., 2016), ResNeXt-101 (Xie et al., 2017) and EfficientNet (Tan and Le, 2019). ResNet (He et al., 2016) is a classical backbone that have been used in many applications and usually used to evaluate many plug-and-play algorithms. ResNet could be defined by different layers, such as ResNet-50 and ResNet-101. ResNeXt-101 (Xie et al., 2017) is constructed by repeating a building block that aggregates a set of transformations with the same topology, which results in a homogeneous, multi-branch architecture that has only a few hyper-parameters to set. EfficientNet (Tan and Le, 2019) is designed by neural architecture search, using a new scaling method that uniformly scales all dimensions of depth, width and resolution using a simple yet highly effective compound coefficient. Table 6 lists the performance (HOS) of all abovementioned network architectures along with different open-set algorithms. Notably, they all belong to plug-and-play algorithms, including our proposed MAOSDAN. Experimental results show that no matter which network architecture is used, our MAOSDAN performs best among different open-set algorithms, which can prove its generalization and versatility.

This paper focuses on open-set domain adaptation for remote sensing images, where there is a partial overlap between the label space

Table 7
Comparisons the performance (%) of HOS among different image degradations (including Gaussian noise and random occlusion) for our proposed MAOSDAN.

Image Degradation	A → N	A → U	N → A	U → A	U → N	Avg
Plain	**73.84**	**79.17**	**82.23**	**74.87**	**65.26**	**75.07**
Gaussian Noise (5%)	71.67	76.11	80.95	72.69	64.83	73.25
Gaussian Noise (10%)	69.86	77.65	78.89	73.81	63.00	72.64
Random Occlusion (10 × 10 pixels)	65.94	76.86	79.29	70.56	63.86	71.30
Random Occlusion (20 × 20 pixels)	64.75	76.42	78.38	69.29	63.29	70.43

Table 8
Accuracy (%) for all the classes on Office-31 (Saenko et al., 2010) for open-set domain adaptation scenarios (ResNet-50).

Method		A→D	A→W	D→A	D→W	W→A	W→D	Avg
ResNet-50		85.2	82.5	71.6	94.1	75.5	96.6	84.2
Standard domain adaptation	DANN	86.5	85.3	75.7	97.5	74.9	99.5	86.60
	RTN	89.5	85.6	72.3	94.8	73.5	97.1	85.4
Open-set domain adaptation	ATI	84.3	87.4	78.0	93.6	80.4	96.5	86.7
	OSBP	88.6	86.5	88.9	97.0	85.8	97.9	90.8
	STA	**93.7**	89.5	89.1	97.5	87.9	**99.5**	92.9
	Ours	93.2	**90.4**	**90.6**	**98.3**	87.4	**99.5**	**93.2**

Table 9
Accuracy (%) for all the classes on Office-Home (Venkateswara et al., 2017) for open-set domain adaptation scenarios (ResNet-50).

Method		A→C	A→P	A→R	C→A	C→P	C→R	P→A	P→C	P→R	R→A	R→C	R→P	Avg
ResNet-50		53.4	69.3	78.7	61.4	61.8	71.0	64.0	52.7	74.9	70.0	51.9	74.1	65.3
Standard domain adaptation	DANN	54.6	69.5	80.2	61.9	63.5	71.7	63.3	49.7	74.2	71.3	51.9	72.9	65.4
	CDAN	54.4	67.0	78.2	62.0	62.7	70.9	61.9	50.8	74.8	69.1	51.6	72.4	64.6
Open-set domain adaptation	ATI	55.2	69.1	79.2	61.7	63.5	72.9	64.5	52.6	75.8	70.7	53.5	74.1	66.1
	OSBP	56.7	67.5	80.6	62.5	65.5	74.7	64.8	51.5	71.5	69.3	49.2	74.0	65.7
	STA	58.1	**71.6**	85.0	63.4	69.3	75.8	65.2	53.1	**80.8**	**74.9**	54.4	**81.9**	69.5
	Ours	**62.1**	69.3	**85.2**	**65.5**	**69.6**	**76.2**	**65.3**	**59.2**	80.4	74.8	**56.0**	81.0	**70.4**

of the target domain and that of the source domain. Since this paper design a new algorithm to transfer knowledge across different domains, our proposed method could tackle multi-sensor, multi-temporal or cross-regional remote sensing scenarios as they do not rely on labels or annotations in the target domain. Our proposed method (i.e., MAOSDAN) tries to address the various conditions, such as different resolutions, different sensors, different locations and different photographing time, etc. To this end, our proposed method is robust to meet various changing conditions for remote sensing images classification. On the other hand, we have also added experiments about performance of our proposed MAOSDAN under different image degradations including adding noises and occlusions. We add Gaussian noise (5% and 10%) and random black occlusions with 10 × 10 pixels and 20 × 20 pixels. Notably, we only conduct image degradation for target domain, which could evaluate the method's capacity of meeting the various variabilities and occlusions. From Table 7, we observe that even though we add different level degradations for images, the performance degradations are lower than 5%, indicating that our proposed MAOSDAN has strong robustness and generalization to overcome the various variabilities and occlusions.

6.3. The performance of MAOSDAN on standard open-set DA datasets

We also validate MAOSDAN on standard open-set DA datasets, such as Office-Home (Peng et al., 2019) and Office-31 (Saenko et al., 2010), which is listed in Table 8 and 9. Office-31 consists of 31 classes in 3 domains: Webcam (W), DSLR (D) and Amazon (A). Similar to the same data protocol in previous open-set DA publications (Saito et al., 2018), the classes with labels 11–31 in alphabetical order are recognized as "unknown" classes in the target domain. Office-Home (Venkateswara et al., 2017) is a larger-scale challenging domain adaptation dataset than Office-31. There are four domains (Art (A), Clipart (C), Product (P) and Real-World (R)) with 65 classes. We follow Liu et al. (2019) to construct the target domain using the first 40 categories in alphabetical order, where the first 25 classes in alphabetic order are recognized as known classes and the remaining 40 classes are recognized as "unknown" class. As listed in Tables 8 and 9, our proposed MAOSDAN yields highest average accuracy in both two standard open-set DA dataset, *i.e.*, Office-Home and Office-31, indicating that our MAOSDAN is more robust and effective than other state-of-the-art open-set DA approaches.

6.4. Feature visualization

In Fig. 7, we present the visualizations of network features extracted from the final convolutional layer for three different transfer tasks: **A** → **U**, **N** → **A**, and **U** → **A**. In domain adaptation scenarios, we strive to transfer the knowledge from the source domain (with labels) to the target domain (without labels), and only focus on the performance for the target domain. Therefore, we only visualize the feature distribution for the target domain using t-SNE, which is consistent to existing studies (Lin et al., 2020; Makkar et al., 2021; Bai et al., 2022). These visualizations showcase the feature transferability of ResNet-50 (Baseline), DAN, OSBP, and our proposed method MAOSDAN (Ours) using the t-SNE visualization technique (Van der Maaten and Hinton, 2008; Donahue et al., 2014). The visualization illustrates the "unknown" classes in an open-set domain adaptation scenario. The yellow points represent these "unknown" classes. It is evident from the visualization that as we progress from the ResNet-50 model on the left to our proposed MAOSDAN model on the right, the target domain samples become increasingly difficult to distinguish. Specifically, in the transfer task from **A** to **U**, the features generated by MAOSDAN exhibit 14 distinct clusters with well-defined boundaries. In addition, we can observe that open set DA methods considerably performs better closed set DA approaches in general. The improved visual performance exhibited by MAOSDAN demonstrates the efficacy of our novel algorithms in generating highly transferable representations and mitigating the adverse effects of negative transfer in open-set domain adaptation scenarios.

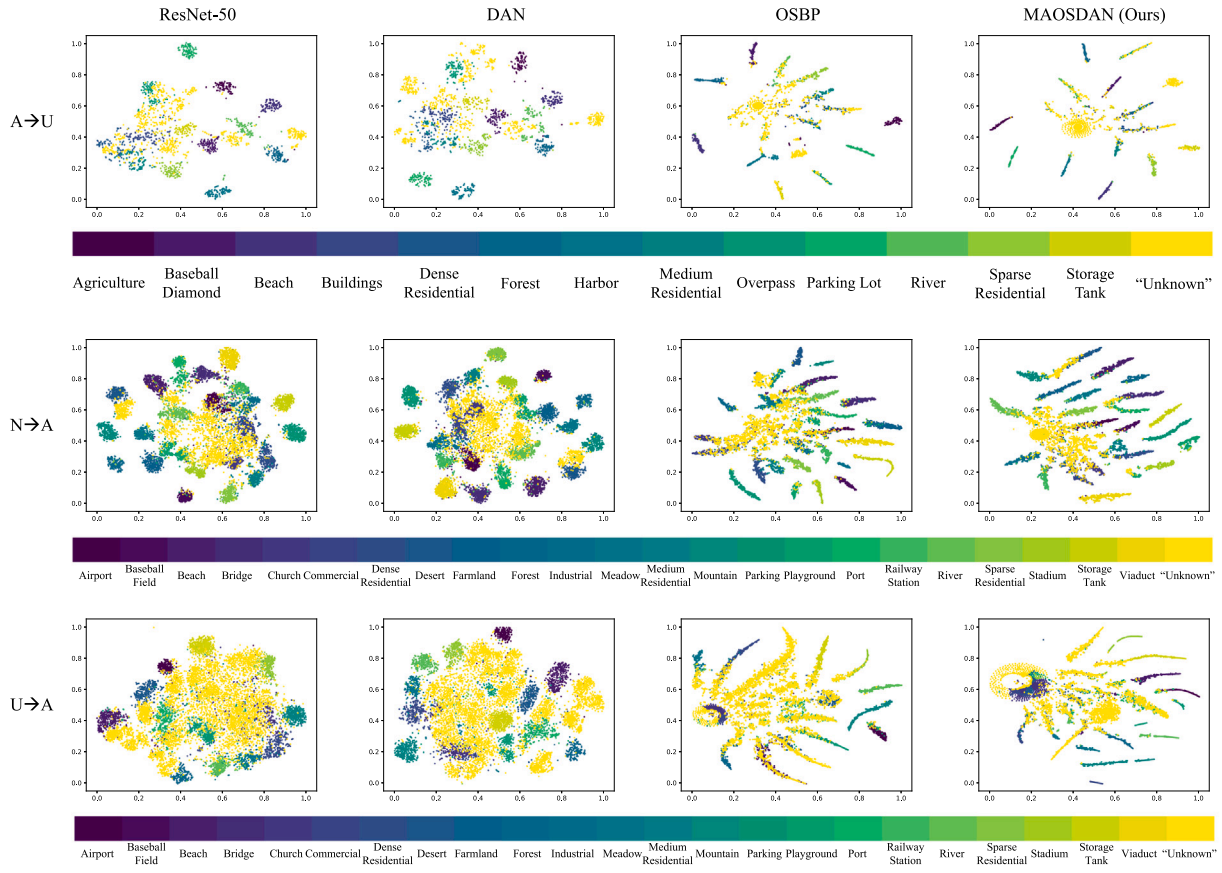

Fig. 7. The t-SNE visualization of features for three transfer tasks (from top to bottom: **A** → **U**, **N** → **A** and **U** → **A**) learned by the Baseline (ResNet-50), DAN, OSBP and MAOSDAN (Ours) (from left to right). (For interpretation of the references to color in this figure legend, the reader is referred to the web version of this article.)

6.5. Potential practical application scenarios in the remote sensing community leveraging MAOSDAN

Open-set DA issue is a more challenging and practical task in transfer learning. While the domain adaptation problem has been extensively explored and examined in the context of remote sensing image classification in recent years, there is a lack of empirical studies that specifically address the situation where the label set of the target domain includes that of the source domain. Nevertheless, it is common to encounter situations regarding remote sensing fields where transferring our model to a new dataset that may include novel classes that were not seen during the training phase is necessary. Utilizing conventional DA methods without proper considerations may lead to negative transfer effects when dealing with "unknown" classes in the target domain, as the label distributions between the source and target domains are disjoint. This mismatch can significantly deteriorate the transferability of the model and impede its performance.

For instance, if we are supposed to conduct tree species classification using remote sensing images (or forest inventory), in which few people have been gone there, obviously, determining the precise tree species beforehand is an insurmountable challenge for us. In addition, the data-bank of tree species from other regions may not include all the tree species in the target domain, where there probably exist brand new tree species. Hence, we employ open-set DA techniques to identify the tree species in the underpopulated forest. This approach eliminates the need for additional annotations and human interpretation, as well as mitigates the adverse effects of negative transfer that typically arise from conventional DA methods. On the other hand, when conducting land cover and land use mapping, it is common to collect samples of various types in metropolitan areas like Shanghai and New York. However, when attempting to transfer this knowledge to micropolitan areas such as Kashgar and Anchorage, new land cover and land use types may emerge that were not present in the metropolitan areas. These new types, such as desert and tundra, introduce unique challenges in the mapping process. Therefore, recognizing these "unknown" classes is quite vital in remote sensing applications and open set DA algorithm can help us to better tackle this issue.

In addition, gathering samples for the target domain is a challenging and resource-intensive task, requiring significant time and effort. Additionally, obtaining accurate information regarding the precise label set of the target domain can be elusive. To this end, our MAOSDAN algorithm fills a crucial gap in the field of open-set domain adaptation for scene classification in remote sensing images. In contrast to existing DA algorithms, MAOSDAN offers effective solutions to mitigate the negative transfer effect caused by the presence of "unknown" classes in the target domain. Additionally, MAOSDAN demonstrates superior performance in accurately distinguishing between "known" and "unknown" classes. In contrast to other existing open-set domain adaptation algorithms, our proposed MAOSDAN demonstrates superior performance across standard domain adaptation datasets. This significant improvement establishes MAOSDAN as a robust and practical method that holds great promise in both the computer vision and remote sensing communities.

6.6. Limitations and future works

MAOSDAN is an encouraging domain adaptation method that demonstrates highly promising results not only for transferring the source domain knowledge to the target domain without annotations, but also for scenarios where the label set of the source domain is a subset of the target domain. However, our proposed MAOSDAN and the experimental results introduced in Section 5 still exist some limitations and could be further improved.

1. From the perspective of data, we only adopt RGB-band satellite images in this paper and only capture the visible representative features and texture. Given the limitation of the visible-band-only images in remote sensing applications, we will evaluate our proposed MAOSDAN for other typical kinds of remote sensing images, such as multi-spectral or hyper-spectral images, which may exploit the inherent properties among the different geo-objects. Also, as our MAOSDAN is a plug-and-play algorithm that could easily applied to other network architectures and other kinds of data, we will try to applied our MAOSDAN to 3D point cloud data for segmentation or detection tasks, or long-time-series data for time series analysis in the future.
2. From the perspective of methodology, existing open-set domain adaptation methods focus on exploring novel samples to achieve "known" and "unknown" separation ("unknown" class detection) and adapting the "known" class distribution (domain alignment). Including our proposed MAOSDAN, most of existing open-set domain adaptation methods only consider "known" class semantics in the source domain, while ignoring the "unknown" class spreading everywhere. This leads to a semantic-level bias between the "known" and "unknown" class, further yielding a biased domain transfer for open-set domain adaptation. In the future, we will observe and formulate the ever-overlooked semantic-level bias and make more improvements for open-set domain adaptation scenarios.
3. From the perspective of transfer paradigm, we only consider the open-set domain adaptation scenario, where the label set of source domain is a subset of that of target domain, which means there exists "unknown" class in the target domain. Some researchers have also exploited the partial domain adaptation scenarios (Hu et al., 2020; Zheng et al., 2022), where the label set of target domain is a subset of that of source domain, which means there exists outlier class in the source domain. Furthermore, universal domain adaptation scenario (Xu et al., 2023) generalizes above two settings, where the source and target domains usually share some labels, but at the same time each has a private set of labels that the other does not have, which is not restricted to any prior knowledge. To this end, we will explore the more challenging domain adaptation scenarios and utilize the strategies from MAOSDAN to new transfer tasks.

7. Conclusion

In this paper, we introduce a novel approach called MAOSDAN (Multi-Adversarial Open-Set Domain Adaptation Network) for scene classification in the field of remote sensing. Our algorithm addresses the challenge of partial label set overlap between the target and source domains in domain adaptation scenarios. Our MAOSDAN consists of three major components. First, we employ an attention-aware OSBP to better distinguish the "unknown" and "known" samples for the target domain. Second, we design an auxiliary adversarial learning to prevent from the negative transfer effect caused by forcefully aligning the "unknown" target sample by a threshold as most existing open-set DA approaches. Finally, we adopt an adaptive entropy suppression to increase the probability of samples and prevent some samples from being mistakenly classified (such as "unknown" target samples). To alleviate forceful entropy minimization, it also alleviates those difficult to distinguish as "known" or "unknown" samples to be mistakenly classified. To evaluate the effectiveness of our proposed MAOSDAN, we conducted experiments using a test dataset comprising three publicly available remote sensing datasets: NWPU-RESISC45, AID, and UC Merced. Our method achieved an average HOS of 75.07%, surpassing other existing open-set DA approaches by an average HOS improvement ranging from 4.52% to 17.15%. Moreover, our method outperformed the baseline CNN model by a significant margin, demonstrating a substantial gain of 18.12% in performance. Our experimental findings demonstrate that our proposed MAOSDAN method exhibits significant promise in tackling a practical and widely applicable challenge, specifically when the target domain comprises samples from classes that are not present in the source domain. In our future research, we aim to investigate the capabilities of our MAOSDAN in real-world open-set domain adaptation scenarios, specifically focusing on applications in the remote sensing domain. These scenarios will involve diverse challenges such as limited annotations, multi-temporal data, multiple sensors, and various regions. Some of the specific applications we plan to explore include tree species classification, land cover mapping, and land use mapping. By addressing these practical challenges, we hope to further validate and extend the effectiveness of MAOSDAN in real-world settings.

Declaration of competing interest

The authors declare that they have no known competing financial interests or personal relationships that could have appeared to influence the work reported in this paper.

Acknowledgments

This research was supported in part by the National Natural Science Foundation of China (Grant No. T2125006 and 42201358), and the Jiangsu Innovation Capacity Building Program (Grant No. BM2022 028).

References

Adayel, R., Bazi, Y., Alhichri, H., Alajlan, N., 2020. Deep open-set domain adaptation for cross-scene classification based on adversarial learning and pareto ranking. Rem. Sens. 12 (11), 1716.

Bai, L., Du, S., Zhang, X., Wang, H., Liu, B., Ouyang, S., 2022. Domain adaptation for remote sensing image semantic segmentation: An integrated approach of contrastive learning and adversarial learning. IEEE Trans. Geosci. Remote Sens. 60, 1–13.

Bottou, L., 2010. Large-scale machine learning with stochastic gradient descent. In: Proceedings of COMPSTAT'2010. Springer, pp. 177–186.

Bousmalis, K., Trigeorgis, G., Silberman, N., Krishnan, D., Erhan, D., 2016. Domain separation networks. In: Advances in neural information processing systems, vol.29, pp. 343–351.

Bucci, S., Loghmani, M.R., Tommasi, T., 2020. On the effectiveness of image rotation for open set domain adaptation. In: European Conference on Computer Vision. Springer, pp. 422–438.

Cao, Z., Ma, L., Long, M., Wang, J., 2018. Partial adversarial domain adaptation. In: Proceedings of the European Conference on Computer Vision. ECCV, pp. 135–150.

Cao, Z., You, K., Long, M., Wang, J., Yang, Q., 2019. Learning to transfer examples for partial domain adaptation. In: Proceedings of the IEEE/CVF Conference on Computer Vision and Pattern Recognition. pp. 2985–2994.

Carlucci, F.M., D'Innocente, A., Bucci, S., Caputo, B., Tommasi, T., 2019. Domain generalization by solving Jigsaw puzzles. In: Proceedings of the IEEE/CVF Conference on Computer Vision and Pattern Recognition. pp. 2229–2238.

Chen, L., Chen, H., Wei, Z., Jin, X., Tan, X., Jin, Y., Chen, E., 2022. Reusing the task-specific classifier as a discriminator: Discriminator-free adversarial domain adaptation. In: Proceedings of the IEEE/CVF Conference on Computer Vision and Pattern Recognition. pp. 7181–7190.

Chen, J., Wang, X., 2022. Open set few-shot remote sensing scene classification based on a multi-order graph convolutional network and domain adaptation. IEEE Trans. Geosci. Remote Sens..

Cheng, G., Han, J., Lu, X., 2017. Remote sensing image scene classification: Benchmark and state of the art. Proc. IEEE 105 (10), 1865–1883.

Donahue, J., Jia, Y., Vinyals, O., Hoffman, J., Zhang, N., Tzeng, E., Darrell, T., 2014. Decaf: A deep convolutional activation feature for generic visual recognition. In: International Conference on Machine Learning. PMLR, pp. 647–655.

Donahue, J., Krähenbühl, P., Darrell, T., 2016. Adversarial feature learning. arXiv preprint arXiv:1605.09782.

Elshamli, A., Taylor, G.W., Areibi, S., 2019. Multisource domain adaptation for remote sensing using deep neural networks. IEEE Trans. Geosci. Remote Sens. 58 (5), 3328–3340.

Feng, Q., Kang, G., Fan, H., Yang, Y., 2019. Attract or distract: Exploit the margin of open set. In: Proceedings of the IEEE/CVF International Conference on Computer Vision. pp. 7990–7999.

Ganin, Y., Ustinova, E., Ajakan, H., Germain, P., Larochelle, H., Laviolette, F., Marchand, M., Lempitsky, V., 2016. Domain-adversarial training of neural networks. J. Mach. Learn. Res. 17 (1), 2030–2096.

Ghifary, M., Kleijn, W.B., Zhang, M., Balduzzi, D., Li, W., 2016. Deep reconstruction-classification networks for unsupervised domain adaptation. In: European Conference on Computer Vision. Springer, pp. 597–613.

Goodfellow, I.J., Pouget-Abadie, J., Mirza, M., Xu, B., Warde-Farley, D., Ozair, S., Courville, A., Bengio, Y., 2014. Generative adversarial nets. In: Proceedings of the 27th International Conference on Neural Information Processing Systems-Volume 2. pp. 2672–2680.

Grandvalet, Y., Bengio, Y., 2004. Semi-supervised learning by entropy minimization. In: Proceedings of the 17th International Conference on Neural Information Processing Systems. pp. 529–536.

He, K., Zhang, X., Ren, S., Sun, J., 2016. Deep residual learning for image recognition. In: Proceedings of the IEEE Conference on Computer Vision and Pattern Recognition. pp. 770–778.

Hong, D., Gao, L., Yokoya, N., Yao, J., Chanussot, J., Du, Q., Zhang, B., 2020. More diverse means better: Multimodal deep learning meets remote-sensing imagery classification. IEEE Trans. Geosci. Remote Sens. 59 (5), 4340–4354.

Hou, D., Wang, S., Tian, X., Xing, H., 2022. PCLUDA: A pseudo-label consistency learning-based unsupervised domain adaptation method for cross-domain optical remote sensing image retrieval. IEEE Trans. Geosci. Remote Sens. 61, 1–14.

Hu, J., Tuo, H., Wang, C., Zhong, H., Pan, H., Jing, Z., 2020. Unsupervised satellite image classification based on partial transfer learning. Aerosp. Syst. 3 (1), 21–28.

Huang, W., Shi, Y., Xiong, Z., Wang, Q., Zhu, X.X., 2023. Semi-supervised bidirectional alignment for remote sensing cross-domain scene classification. ISPRS J. Photogramm. Remote Sens. 195, 192–203.

Iqbal, J., Ali, M., 2020. Weakly-supervised domain adaptation for built-up region segmentation in aerial and satellite imagery. ISPRS J. Photogramm. Remote Sens. 167, 263–275.

Jang, J., Na, B., Shin, D.H., Ji, M., Song, K., Moon, I.-C., 2022. Unknown-aware domain adversarial learning for open-set domain adaptation. Adv. Neural Inf. Process. Syst. 35, 16755–16767.

Jing, M., Li, J., Zhu, L., Ding, Z., Lu, K., Yang, Y., 2021. Balanced open set domain adaptation via centroid alignment. In: Proceedings of the AAAI Conference on Artificial Intelligence. Vol. 35, no. 9. pp. 8013–8020.

Kalita, I., Roy, M., 2020. Deep neural network-based heterogeneous domain adaptation using ensemble decision making in land cover classification. IEEE Trans. Artif. Intell. 1 (2), 167–180.

Kishida, I., Chen, H., Baba, M., Jin, J., Amma, A., Nakayama, H., 2021. Object recognition with continual open set domain adaptation for home robot. In: Proceedings of the IEEE/CVF Winter Conference on Applications of Computer Vision. pp. 1517–1526.

Koga, Y., Miyazaki, H., Shibasaki, R., 2020. A method for vehicle detection in high-resolution satellite images that uses a region-based object detector and unsupervised domain adaptation. Remote Sens. 12 (3), 575.

Kussul, N., Lavreniuk, M., Skakun, S., Shelestov, A., 2017. Deep learning classification of land cover and crop types using remote sensing data. IEEE Geosci. Remote Sens. Lett. 14 (5), 778–782.

Li, X., Luo, M., Ji, S., Zhang, L., Lu, M., 2020a. Evaluating generative adversarial networks based image-level domain transfer for multi-source remote sensing image segmentation and object detection. Int. J. Remote Sens. 41 (19), 7343–7367.

Li, Y., Shi, T., Zhang, Y., Chen, W., Wang, Z., Li, H., 2021. Learning deep semantic segmentation network under multiple weakly-supervised constraints for cross-domain remote sensing image semantic segmentation. ISPRS J. Photogramm. Remote Sens. 175, 20–33.

Li, K., Wan, G., Cheng, G., Meng, L., Han, J., 2020b. Object detection in optical remote sensing images: A survey and a new benchmark. ISPRS J. Photogramm. Remote Sens. 159, 296–307.

Lin, J., Yu, T., Mou, L., Zhu, X., Ward, R.K., Wang, Z.J., 2020. Unifying top-down views by task-specific domain adaptation. IEEE Trans. Geosci. Remote Sens..

Liu, H., Cao, Z., Long, M., Wang, J., Yang, Q., 2019. Separate to adapt: Open set domain adaptation via progressive separation. In: Proceedings of the IEEE/CVF Conference on Computer Vision and Pattern Recognition. pp. 2927–2936.

Liu, W., Su, F., 2020. A novel unsupervised adversarial domain adaptation network for remotely sensed scene classification. Int. J. Remote Sens. 41 (16), 6099–6116.

Liu, W., Wang, Z., Liu, X., Zeng, N., Liu, Y., Alsaadi, F.E., 2017. A survey of deep neural network architectures and their applications. Neurocomputing 234, 11–26.

Loghmani, M.R., Vincze, M., Tommasi, T., 2020. Positive-unlabeled learning for open set domain adaptation. Pattern Recognit. Lett. 136, 198–204.

Long, M., Cao, Y., Wang, J., Jordan, M., 2015. Learning transferable features with deep adaptation networks. In: International Conference on Machine Learning. PMLR, pp. 97–105.

Long, M., Cao, Z., Wang, J., Jordan, M.I., 2018. Conditional adversarial domain adaptation. In: Proceedings of the 32nd International Conference on Neural Information Processing Systems. pp. 1647–1657.

Long, M., Zhu, H., Wang, J., Jordan, M.I., 2016. Unsupervised domain adaptation with residual transfer networks. In: Proceedings of the 30th International Conference on Neural Information Processing Systems. pp. 136–144.

Long, M., Zhu, H., Wang, J., Jordan, M.I., 2017. Deep transfer learning with joint adaptation networks. In: International Conference on Machine Learning. PMLR, pp. 2208–2217.

Lu, X., Gong, T., Zheng, X., 2019. Multisource compensation network for remote sensing cross-domain scene classification. IEEE Trans. Geosci. Remote Sens. 58 (4), 2504–2515.

Lu, X., Zhong, Y., Zheng, Z., Wang, J., 2021. Cross-domain road detection based on global-local adversarial learning framework from very high resolution satellite imagery. ISPRS J. Photogramm. Remote Sens. 180, 296–312.

Luo, M., Ji, S., 2022. Cross-spatiotemporal land-cover classification from VHR remote sensing images with deep learning based domain adaptation. ISPRS J. Photogramm. Remote Sens. 191, 105–128.

Ma, X., Mou, X., Wang, J., Liu, X., Geng, J., Wang, H., 2020. Cross-dataset hyperspectral image classification based on adversarial domain adaptation. IEEE Trans. Geosci. Remote Sens..

Makkar, N., Yang, L., Prasad, S., 2021. Adversarial learning based discriminative domain adaptation for geospatial image analysis. IEEE J. Sel. Top. Appl. Earth Obs. Remote Sens. 15, 150–162.

Mateo-García, G., Laparra, V., López-Puigdollers, D., Gómez-Chova, L., 2020. Transferring deep learning models for cloud detection between Landsat-8 and Proba-V. ISPRS J. Photogramm. Remote Sens. 160, 1–17.

Mirza, M., Osindero, S., 2014. Conditional generative adversarial nets. arXiv preprint arXiv:1411.1784.

Niu, B., Pan, Z., Chen, K., Hu, Y., Lei, B., 2023. Open set domain adaptation via instance affinity metric and fine-grained alignment for remote sensing scene classification. IEEE Geosci. Remote Sens. Lett..

Nyborg, J., Pelletier, C., Lefèvre, S., Assent, I., 2022. TimeMatch: Unsupervised cross-region adaptation by temporal shift estimation. ISPRS J. Photogramm. Remote Sens. 188, 301–313.

Pan, S.J., Yang, Q., 2009. A survey on transfer learning. IEEE Trans. Knowl. Data Eng. 22 (10), 1345–1359.

Pan, Y., Yao, T., Li, Y., Ngo, C.-W., Mei, T., 2020. Exploring category-agnostic clusters for open-set domain adaptation. In: Proceedings of the IEEE/CVF Conference on Computer Vision and Pattern Recognition. pp. 13867–13875.

Panareda Busto, P., Gall, J., 2017. Open set domain adaptation. In: Proceedings of the IEEE International Conference on Computer Vision. pp. 754–763.

Paszke, A., Gross, S., Massa, F., Lerer, A., Bradbury, J., Chanan, G., Killeen, T., Lin, Z., Gimelshein, N., Antiga, L., et al., 2019. PyTorch: An imperative style, high-performance deep learning library. In: Advances in Neural Information Processing Systems. pp. 8024–8035.

Peng, X., Bai, Q., Xia, X., Huang, Z., Saenko, K., Wang, B., 2019. Moment matching for multi-source domain adaptation. In: Proceedings of the IEEE/CVF International Conference on Computer Vision. pp. 1406–1415.

Rakshit, S., Tamboli, D., Meshram, P.S., Banerjee, B., Roig, G., Chaudhuri, S., 2020. Multi-source open-set deep adversarial domain adaptation. In: European Conference on Computer Vision. Springer, pp. 735–750.

Russakovsky, O., Deng, J., Su, H., Krause, J., Satheesh, S., Ma, S., Huang, Z., Karpathy, A., Khosla, A., Bernstein, M., et al., 2015. Imagenet large scale visual recognition challenge. Int. J. Comput. Vis. 115 (3), 211–252.

Saenko, K., Kulis, B., Fritz, M., Darrell, T., 2010. Adapting visual category models to new domains. In: European Conference on Computer Vision. Springer, pp. 213–226.

Saito, K., Yamamoto, S., Ushiku, Y., Harada, T., 2018. Open set domain adaptation by backpropagation. In: Proceedings of the European Conference on Computer Vision. ECCV, pp. 153–168.

Shamsolmoali, P., Zareapoor, M., Zhou, H., Wang, R., Yang, J., 2020. Road segmentation for remote sensing images using adversarial spatial pyramid networks. IEEE Trans. Geosci. Remote Sens..

Shen, S., Xia, Y., Eich, A., Xu, Y., Yang, B., Stilla, U., 2023. SegTrans: Semantic segmentation with transfer learning for MLS point clouds. IEEE Geosci. Remote Sens. Lett..

Shermin, T., Lu, G., Teng, S.W., Murshed, M., Sohel, F., 2020. Adversarial network with multiple classifiers for open set domain adaptation. IEEE Trans. Multimed..

Sun, B., Feng, J., Saenko, K., 2016. Return of frustratingly easy domain adaptation. In: Proceedings of the AAAI Conference on Artificial Intelligence. Vol. 30, no. 1.

Tan, M., Le, Q., 2019. Efficientnet: Rethinking model scaling for convolutional neural networks. In: International Conference on Machine Learning. PMLR, pp. 6105–6114.

Tuia, D., Marcos, D., Camps-Valls, G., 2016a. Multi-temporal and multi-source remote sensing image classification by nonlinear relative normalization. ISPRS J. Photogramm. Remote Sens. 120, 1–12.

Tuia, D., Persello, C., Bruzzone, L., 2016b. Domain adaptation for the classification of remote sensing data: An overview of recent advances. IEEE Geosci. Rem. Sens. Mag. 4 (2), 41–57.

Van der Maaten, L., Hinton, G., 2008. Visualizing data using t-SNE. J. Mach. Learn. Res. 9 (11).

Vega, P.J.S., da Costa, G.A.O.P., Feitosa, R.Q., Adarme, M.X.O., de Almeida, C.A., Heipke, C., Rottensteiner, F., 2021. An unsupervised domain adaptation approach for change detection and its application to deforestation mapping in tropical biomes. ISPRS J. Photogramm. Remote Sens. 181, 113–128.

Venkateswara, H., Eusebio, J., Chakraborty, S., Panchanathan, S., 2017. Deep hashing network for unsupervised domain adaptation. In: Proceedings of the IEEE Conference on Computer Vision and Pattern Recognition. pp. 5018–5027.

Wang, S., Hou, D., Xing, H., 2023. A self-supervised-driven open-set unsupervised domain adaptation method for optical remote sensing image scene classification and retrieval. IEEE Trans. Geosci. Remote Sens. 61, 1–15.

Wang, Q., Huang, W., Xiong, Z., Li, X., 2020. Looking closer at the scene: Multiscale representation learning for remote sensing image scene classification. IEEE Trans. Neural Netw. Learn. Syst..

Wittich, D., Rottensteiner, F., 2021. Appearance based deep domain adaptation for the classification of aerial images. ISPRS J. Photogramm. Remote Sens. 180, 82–102.

Wu, W., Zheng, J., Fu, H., Li, W., Yu, L., 2020. Cross-regional oil palm tree detection. In: Proceedings of the IEEE/CVF Conference on Computer Vision and Pattern Recognition Workshops. pp. 56–57.

Xia, G.-S., Hu, J., Hu, F., Shi, B., Bai, X., Zhong, Y., Zhang, L., Lu, X., 2017. AID: A benchmark data set for performance evaluation of aerial scene classification. IEEE Trans. Geosci. Remote Sens. 55 (7), 3965–3981.

Xie, S., Girshick, R., Dollár, P., Tu, Z., He, K., 2017. Aggregated residual transformations for deep neural networks. In: Proceedings of the IEEE Conference on Computer Vision and Pattern Recognition. pp. 1492–1500.

Xu, K., Huang, H., Deng, P., Li, Y., 2021. Deep feature aggregation framework driven by graph convolutional network for scene classification in remote sensing. IEEE Trans. Neural Netw. Learn. Syst..

Xu, R., Li, G., Yang, J., Lin, L., 2019. Larger norm more transferable: An adaptive feature norm approach for unsupervised domain adaptation. In: Proceedings of the IEEE/CVF International Conference on Computer Vision. pp. 1426–1435.

Xu, Q., Shi, Y., Yuan, X., Zhu, X.X., 2023. Universal domain adaptation for remote sensing image scene classification. IEEE Trans. Geosci. Remote Sens. 61, 1–15.

Yang, Y., Newsam, S., 2010. Bag-of-visual-words and spatial extensions for land-use classification. In: Proceedings of the 18th SIGSPATIAL International Conference on Advances in Geographic Information Systems. pp. 270–279.

Ye, M., Qian, Y., Zhou, J., Tang, Y.Y., 2017. Dictionary learning-based feature-level domain adaptation for cross-scene hyperspectral image classification. IEEE Trans. Geosci. Remote Sens. 55 (3), 1544–1562.

Zhang, H., Chen, D., Liu, L., 2020. Learning likelihood estimates for open set domain adaptation. In: 2020 IEEE International Conference on Multimedia and Expo. ICME, IEEE, pp. 1–6.

Zhang, J., Liu, J., Pan, B., Chen, Z., Xu, X., Shi, Z., 2021a. An open set domain adaptation algorithm via exploring transferability and discriminability for remote sensing image scene classification. IEEE Trans. Geosci. Remote Sens..

Zhang, R., Newsam, S., Shao, Z., Huang, X., Wang, J., Li, D., 2021b. Multi-scale adversarial network for vehicle detection in UAV imagery. ISPRS J. Photogramm. Remote Sens. 180, 283–295.

Zhang, X., Yao, X., Feng, X., Cheng, G., Han, J., 2021c. DFENet for domain adaptation based remote sensing scene classification. IEEE Trans. Geosci. Remote Sens..

Zheng, J., Fu, H., Li, W., Wu, W., Yu, L., Yuan, S., Tao, W.Y.W., Pang, T.K., Kanniah, K.D., 2021a. Growing status observation for oil palm trees using unmanned aerial vehicle (UAV) images. ISPRS J. Photogramm. Remote Sens. 173, 95–121.

Zheng, J., Fu, H., Li, W., Wu, W., Zhao, Y., Dong, R., Yu, L., 2020. Cross-regional oil palm tree counting and detection via a multi-level attention domain adaptation network. ISPRS J. Photogramm. Remote Sens. 167, 154–177.

Zheng, J., Wu, W., Yuan, S., Fu, H., Li, W., Yu, L., 2021b. Multisource-domain generalization-based oil palm tree detection using very-high-resolution (VHR) satellite images. IEEE Geosci. Remote Sens. Lett..

Zheng, J., Wu, W., Yuan, S., Zhao, Y., Li, W., Zhang, L., Dong, R., Fu, H., 2021c. A two-stage adaptation network (TSAN) for remote sensing scene classification in single-source-mixed-multiple-target domain adaptation (S^2M^2T DA) scenarios. IEEE Trans. Geosci. Remote Sens..

Zheng, J., Yuan, S., Wu, W., Li, W., Yu, L., Fu, H., Coomes, D., 2023. Surveying coconut trees using high-resolution satellite imagery in remote atolls of the Pacific ocean. Remote Sens. Environ. 287, 113485.

Zheng, J., Zhao, Y., Wu, W., Chen, M., Li, W., Fu, H., 2022. Partial domain adaptation for scene classification from remote sensing imagery. IEEE Trans. Geosci. Remote Sens. 61, 1–17.

Zhu, S., Du, B., Zhang, L., Li, X., 2021. Attention-based multiscale residual adaptation network for cross-scene classification. IEEE Trans. Geosci. Remote Sens..

Zhu, X.X., Tuia, D., Mou, L., Xia, G.-S., Zhang, L., Xu, F., Fraundorfer, F., 2017. Deep learning in remote sensing: A comprehensive review and list of resources. IEEE Geosci. Remote Sens. Mag. 5 (4), 8–36.

Zhu, R., Yan, L., Mo, N., Liu, Y., 2019. Semi-supervised center-based discriminative adversarial learning for cross-domain scene-level land-cover classification of aerial images. ISPRS J. Photogramm. Remote Sens. 155, 72–89.

Zou, X., Cheng, M., Wang, C., Xia, Y., Li, J., 2017. Tree classification in complex forest point clouds based on deep learning. IEEE Geosci. Remote Sens. Lett. 14 (12), 2360–2364.